ABSTRACT

Title of Thesis: SEISMIC DESIGN OPTIMIZATION OF STEEL STRUCTURES USING PARTICLE SWARM ALGORITHM

Parteek Middha, Master of Science, 2017

Directed By: Dr. Brian M. Phillips
Department of Civil and Environmental Engineering

Earthquakes are one of the most devastating and expensive natural disasters in the world. Economical and earthquake-resistant design remains a challenge for structural engineers. This study explores the optimal design of a seismic force resisting steel frame using a population based stochastic algorithm known as Particle Swarm Optimization (PSO). PSO is able to efficiently explore a complex solution space with many design variables and constraints. PSO is also problem independent and can be built around any approach to earthquake design. As a case study, the seismic design of a three-story moment resisting frame is optimized for the linear static, linear dynamic, and nonlinear static analysis methods. An interface was created between MATLAB and OpenSees to link optimization with a well-known and freely available earthquake engineering software. This application is extended to the performance-based design of structures, in which the optimal design meets the target performance objectives of Immediate Occupancy, Life Safety, and Collapse Prevention under Frequent, Design, and Maximum-considered seismic hazard levels.

SEISMIC DESIGN OPTIMIZATION OF STEEL STRUCTURES USING PARTICLE SWARM ALGORITHM

By

Parteek Middha

Thesis submitted to the Faculty of the Graduate School of the
University of Maryland, College Park, in partial fulfillment
of the requirements for the degree of
Master of Science
2017

Advisory Committee:

Dr. Brian M. Phillips
Dr. Mark Austin
Dr. Peter Chang

ACKNOWLEDGEMENTS

I would like to take this opportunity to express my sincere gratitude and appreciation to my advisor, Dr. Brian M. Phillips, for his continued support and guidance throughout my studies. His advice was very crucial for the success of this work and I enjoyed my time working under him. I also thank Dr. Yunfeng Zhang for providing the knowledge and insights in regard to this study. I am grateful to Dr. Mark Austin and Dr. Peter Chang for serving on my committee and for taking out their valuable time to feedback on my work.

My family has been supportive throughout this entire period, for which I thank them. My parents and my brother have been very supportive in every way possible and I dedicate this work to them.

TABLE OF CONTENTS

LIST OF TABLES

LIST OF FIGURES

Chapter 1: Introduction

1.1 Background and Motivation

Statistics show that earthquakes are one of the most significant natural disasters worldwide with most death toll from the year 1980 to 2016 [1]. Japan's 2011 earthquake was estimated to be the deadliest natural disaster in history, resulting in 15,880 fatalities and a total economic loss of $235 billion [2]. The January 17, 1994 Northridge earthquake in Los Angeles, California, was recorded as one of the most expensive natural disasters in the history of U.S., costing more than $40 billion and damaging over 100,000 structures [3]. According to Federal Emergency Management Agency (FEMA), thousands of earthquakes of varying magnitudes occur in the U.S. every year and all U.S. territories are vulnerable to earthquakes. Earthquakes are caused by the movement of tectonic plates beneath the earth's surface, and are therefore inevitable and uncertain by nature. Thus, they can continue to pose a great threat to both human life and the built environment.

In the past fifty years, there has been an unprecedented improvement and advancement in earthquake engineering, including seismology and seismic instrumentation, understanding ultimate behavior of structures, improved building codes and standards, the development of performance-based design methodologies, seismic isolation, and energy dissipation; higher costs associated with the seismic design of structures remain a concern. Poor earthquake-prone regions have a rapidly growing population living in basic shelters than in earthquake-safe buildings, which they can't afford. Thus, an economical design of structures capable of withstanding extreme earthquake events are crucial. As a result, minimizing the cost of structural design has gained

widespread interest lately and has presented an interesting optimization problem for researchers and engineers.

Since most real-world optimization problems are nonlinear and complex by nature, heuristics remain an efficient and powerful tool for solving real-world engineering optimization problems. Heuristics are practical techniques that employs a trial-and-error approach in search for an optimal solution. Although an optimal solution is not guaranteed, the method provides sufficiently good solutions to the problems that are impractical or impossible to solve otherwise. Since 1980s metaheuristic algorithms have gained popularity and are being widely used to solve complex optimization problems. Meta- means “beyond” or “higher level”, so metaheuristics are higher-level problem-independent methods that mimic the best processes in nature including biological systems, and physical and chemical processes; therefore, performing better than simple heuristic methods [4]. Unlike conventional linear programming, they are non-deterministic and derivative-free algorithms that do not rely on gradient information, and generally follow an iterative procedure to solve optimization problems. The two key features of metaheuristics are intensification and diversification [5]. Intensification searches for the best solution in a local region, while diversification controls the exploration of the global search space, so the overall efficiency of an algorithm depends on a good balance between the two [6]. The most popular metaheuristic algorithms available in literature include Simulated Annealing (SA), Genetic Algorithms (GA), Ant Colony Optimization (ACO), Particle Swarm Optimization (PSO), Harmony Search (HS), and Cuckoo Search (CS). However, PSO is the most famous and widely used technique because it is easy to implement, and has been successfully used by many researchers in solving many structural design optimization problems; therefore, this study will only consider the application of PSO.

In the past two decades, metaheuristic methods have been applied to many structural optimization problems. Goldberg and Samtani [7] applied GA to minimize the weight of a 10-bar truss and concluded metaheuristic search methods work well within a reasonable amount of time. Lin and Hajela [8] implemented the same in the optimal design of structural systems with discrete design variables. May and Balling [9] used SA for optimizing a 3-D steel frame. Bland [10] produced the first application of ACO to obtain an optimal configuration of a 25-bar space truss. Lee and Geem [11] introduced Harmony Search methods and applied it to several benchmark structural optimization problems. Later, Kaveh and Talatahari [12] extended this application to optimize rigid steel frames using PSO. Cuckoo Search is a new optimization technique proposed by Yang and Deb [13] that is known to be robust in solving different truss structures. A. Kaveh and Bakhshpoori [14] have successfully applied CS to several types of structures.

A. Kaveh, B. Farahmand Azar, A. Hadidi, F. Rezazadeh Sorochi, and S.Talahari [15] applied ACO and GA to the seismic design optimization of a 3-story and a 9-story steel moment frame subjected to equivalent static loads under Operational (OP), IO (Immediate Occupancy), LS (Life Safety), and Collapse Prevention (CP) seismic hazard levels by using design inter-story drifts as constraints. S. Gholizadeh and E. Salajegeh [16] obtained optimal seismic designs using PSO algorithm for a 10-story steel moment-resisting frame (MRF) under seven earthquake ground motions using approximate linear dynamic procedures. In another recent paper, Kaveh and A. Nasrollahi [17] applied CS algorithm to the performance-based seismic design optimization of steel frames using equivalent static analysis and modal response spectrum analysis by interfacing MATLAB and SAP2000 software to perform parallel computing. However, these studies considered simplified analysis procedures; whereas this thesis develops a technique to perform structural design optimization using improved and advanced analysis procedures.

This thesis develops a technique to implement Particle Swarm Optimization algorithm to the seismic design of steel frames using advanced analysis procedures utilizing a MATLAB-OpenSees interface. The Open System for Earthquake Engineering Simulation, commonly known as OpenSees, is a non-profit open-source finite element software developed by Pacific Earthquake Engineering (PEER) Center and University of California, Berkeley, and has advanced capabilities for modeling and analyzing nonlinear and dynamic response of structures [18]. OpenSees uses Tcl programming language scripts in C++ for finite element model building and analysis. However, this study uses OpenSees Navigator instead, as it offers a graphical user interface (GUI) pre- and post-processing framework for the OpenSees like any other commercial structural analysis and design software.

An existing three-story steel moment-resisting frame (MRF) office building based in Los Angeles, California, was selected as a benchmark structure for this study. ASCE 7-10 and FEMA-356 were the two main design standards used for the analysis of the frame. Three types of analysis procedures are considered in this study in the order of their accuracy in predicting the response of structures under earthquakes: Equivalent Lateral Force Procedure (EFP) analysis, Linear Response Time-History analysis (LD), and Nonlinear Static (NLS) or Pushover analysis. ASCE 7-10 is used for EFP and LD analysis, whereas FEMA 356 is used for the Pushover analysis. The optimal design is obtained and compared for each analysis procedure considered. The design and strength checks for the steel members of the frame are performed as per the AISC Steel Manual and the AISC 318-11 seismic provisions. Similarly, the performance-based design optimization of the frame is performed for Immediate Occupancy (IO), Life Safety (LS), and Collapse Prevention (CP) seismic hazard levels.

Using the optimization framework, the differences in optimal results obtained using EFP, LD, and NLS analysis procedures are evaluated and explained. Additionally, the sensitivity of the optimal results to design selections and assumptions is evaluated. In the course of this study, it was determined that the assumptions made by the above design codes on the use of certain seismic design parameters such as fundamental period, T and effective length factor, K, either contradicted or were unspecified in the above design codes.

1.2 Objectives

The ultimate objective of this study is to optimize the seismic design and the performance-based design of a three-story steel moment-resisting frame using equivalent lateral force (EFP), linear response time-history, and nonlinear static pushover analysis procedures. This optimization framework will enable a sensitivity study on the influence of design method and assumptions on the resulting optimal design. This framework includes the following steps:

1) Develop the PSO algorithm in MATLAB and validate the code by considering an example case study that has been used in a published paper. This includes the optimization of the weight of a 10-bar planar truss structure and a six story steel frame building under gravity loading condition. The PSO results are validated in this step in order to confirm that the developed MATLAB algorithm is fit for the proceeding applications.
2) Build a 2-D finite element model of the benchmark structure in OpenSees, perform modal analysis, and validate the model by comparing the first three natural frequencies to the ones provided in the paper. The objective of this step is to ensure that the OpenSees model is accurate and is fit for performing the seismic analysis procedures.
3) Create an interface between MATLAB and OpenSees. The objective of this step was to develop a technique that enables the automation of the OpenSees analysis. This involves

random generation of the design or member sizes of the structure; prompting OpenSees for performing the analysis of this structure; and then feeding the obtained results in OpenSees back into MATLAB.

4) Perform ASCE 7's equivalent lateral force, linear response time-history, and FEMA 356 nonlinear static analysis procedures and optimize the benchmark structure using PSO algorithm developed in the first step for each of the three analysis procedures considered separately. Compare and summarize the optimal seismic designs of the structure.
5) Perform the performance-based design optimization of the structure for the nonlinear static analysis case, in which the structure is designed for the seismic forces corresponding to the IO, LS, and CP seismic hazard levels.
6) Check sensitivity of the two seismic design parameters specified in the ASCE 7 code for EFP analysis case. In this step, fundamental time-period and effective length factors used in the seismic design are changed and the obtained optimal seismic designs are compared with the original optimization results in step 4.

1.3 Organization of Thesis

This chapter presents background and objectives of this thesis. Chapter 2 begins with describing the theory and concepts of PSO and its application in the optimization of structures. Chapter 2 will also review the current seismic design procedures including capacity design method, ASCE 7's equivalent lateral force procedure, linear response time-history analysis, FEMA 356 nonlinear static pushover analysis, and performance-based design of buildings.

The proceeding chapters commensurate with the objectives or the steps discussed in this chapter. Chapter 3 develops the PSO code in MATLAB and includes two optimization examples of a 10-bar truss structure and a six-story steel rigid frame. In Chapter 4, the OpenSees software is

introduced and a 2-D linear static model of the benchmark structure is built followed by validation of the model by comparing the eigenvalue results. Additionally, a technique to create a MATLAB-OpenSees interface is introduced in this chapter. In Chapter 5, the optimization is performed for the LS, LD, and NLS analysis procedures separately, and the obtained optimal seismic designs are summarized and compared. Similarly, in Chapter 6, the PSO is applied to the performance-based design optimization of the frame using the nonlinear static procedure. In Chapter 7, the sensitivity analysis of the two seismic design parameters is performed by comparing the optimization results with changed parameters to the optimal designs obtained with the previously obtained results for the ASCE 7's equivalent lateral force analysis case. Lastly, summary, conclusions and recommendations for future studies are presented in Chapter 8.

Chapter 2: Literature Review

2.1 Particle Swarm Optimization

Particle Swarm Optimization or PSO is a swarm-intelligence based algorithm that is inspired by the social behavior of animals functioning as a group or a swarm such as birds, fishes, insects, etc. The PSO algorithm was first introduced by Kenny and Eberhart in 1995 [19]. A standard PSO algorithm first initializes a population (swarm) of random solutions (particles). Each particle has its own position and a velocity with which it explores the solution space. Then, using an iterative procedure, each particle moves across the search space looking for a better position, i.e., a position that gives a better objective function value. The movement of particles is guided by a particle's best position encountered thus far, known as the local best position, and by the best position among its neighboring particles or the swarm, known as the global best position. In this way, at every iteration, particles' positions are updated, moving towards a better and better solution until the swarm converges into one best position, which becomes an optimal solution.

The original PSO used an equation (see Eq. 2.1) to calculate the velocity of particle that makes the particle move in the direction based on its own best position and the swarm's best position. Therefore, this equation takes care of how fast or slow a particle should be moving based on how far the current particle (x_j^i) is from its own best location (p^i) and its neighbors' best location (p_j^g). In PSO, c_1 and c_2 are trust parameters that controls the attraction of a particle towards its previous best location and swarm's global best location. Kennedy and Eberhart [19] proposed c_1 and c_2 to be taken as 2. Later, Shi [20] added a weight or inertial factor (w) to this velocity equation to tune the trade-off between the global exploration and the local exploitation of the moving particles. Shi and Eberhart [20] recommended using an inertia weight of $0.8 < w <$

1.4 and shown that a linearly decreasing inertia weight can improve the performance of the PSO significantly It should be noted that c_1 , c_2 and w are problem-dependent parameters and are determined based on experience or guess and check approach for PSO's best performance.

$$v_{j+1}^i = wv_j^i + c_1 r_1 \left(p^i - x_j^i\right) + c_2 r_2 (p_j^g - x_j^i) \quad \text{(Eq. 2.1)}$$

$$x_{j+1}^i = x_j^i + v_{j+1}^i \quad \text{(Eq. 2.2)}$$

Where,

v_{j+1}^i	=	Updated velocity of particle i, at $j+1$ iteration
v_j^i	=	Current Velocity of particle i at jth iteration
r_1 & r_2	=	Uniformly distributed random numbers between the range [0, 1]
w	=	Weight or inertia factor
p^i	=	Previous best position of particle i
x_j^i	=	Current position of particle i at jth iteration
c_1 & c_2	=	PSO trust parameters
p_j^g	=	Global best position of particle i at jth iteration

2.2 Optimization of Steel Structures

The objective function will be the weight of the structure, i.e., obtaining the minimal sectional sizes or cross-sectional area of the members. Thus, the variables for the optimization problem are the member sizes, cross-sectional areas, depending if the variables are discrete or continuous. As seen in Figure 2.1, there are mainly two kinds of regions within the search space, which represents the optimization constraints. First is the variable boundary, which are the minimum or maximum limits for the variables. Second is problem-specific or design constraints which may be displacement limits, stress limits, design strength limits for the members, etc. The

bounded region between these two constraints is the feasible region. It can be safely said that an optimal solution is usually near the feasible boundary.

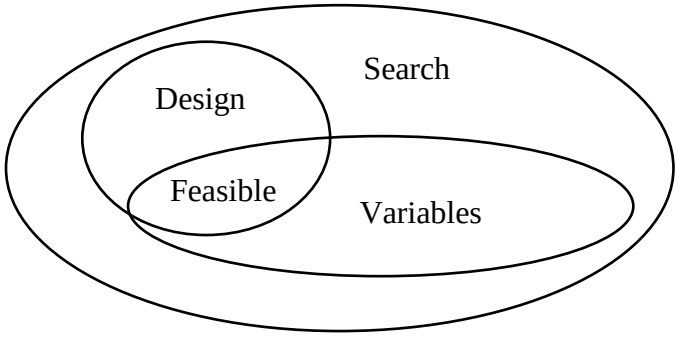

Figure 2.1: Structural Optimization Regions

The general iterative procedure for the PSO optimization can be outlined as follows:

Step 1: Select a swarm size or number of particles of size N, max number of iterations, t_{max}, and PSO parameters $w, c_1, \& \, c_2$ described in the preceding text.

Step 2: Randomly generate particles' positions (X_j^i) within the variables boundary, $[X_{min}, X_{max}]$. where X is a vector of variables for m structural members for i^{th} particle and j^{th} iteration.

Step 3: Randomly initialize particles' velocities (V_j^i) in the range $[-V_{min}, V_{max}]$. Thus, each particle must have its own position and a velocity.

Step 4: Perform the analysis for each particle and determine if the design constraints for that particle are satisfied, if not, regenerate i^{th} particle's position, if yes, evaluate i^{th} objective function and assign this position as $pbest_j^i$ or present best (local best) position. Each particle should have an associated cost, and the best cost among all the particles or swarm becomes the $gbest$.

Step 4: Given $pbest_j^i$, $gbest$, and the PSO parameters, update each particle's velocity and position based on the Eq. 2.1 and Eq. 2.2, respectively.

Step 5: Repeat Step 4, perform the analysis and check all the design constraints for each particle. If the constraints are met, evaluate the objective function and if this cost is better than the previous best cost, $pbest_{j-1}^{i}$, then assign this cost as the particle's new $pbest_{j}^{i}$, and the new $gbest$ is the best of all $pbest_{j}^{i}$. In this way, the $gbest$ gets updated with every iteration.

Step 6: Repeat Steps 4-6 until the termination conditions are met or $j < tmax$, and the optimal solution is the final $gbest$ and its position.

2.2.1 AISC-LRFD Steel Frames

In a typical structural design of an unbraced steel frame, the column and beam sections are selected from the standard steel section tables available in the AISC manual [21]. The most commonly used primary members in the steel frames are W-shapes, taken from a table of 273 W-shape sections available in the AISC manual. These 273 sections can be arranged in a sequence and these 1 to 273 sequence numbers can be treated as discrete design variables. At any stage of optimization, once a sequence number is generated by the algorithm, the real values of the design variable (Area, Moment of Inertia, Self-Weight, etc.) corresponding to this sequence number can be easily taken from the discrete set.

In addition to the displacement constraints, the design of steel frame should include the strength requirements for beams and columns as per the following AISC-LRFD strength check equations for beam-column members:

$$\frac{P_u}{\phi_C P_n} + \frac{8}{9}\frac{M_{u,x}}{\phi_b M_{n,x}} \leq 1.0 \qquad for\ \frac{P_u}{\phi_C P_n} \geq 0.2 \qquad \text{Eq. 2.3}$$

$$\frac{P_u}{2\,\phi_C P_n} + \frac{M_{u,x}}{\phi_b M_{n,x}} \leq 1.0 \qquad for\ \frac{P_u}{\phi_C P_n} \leq 0.2 \qquad \text{Eq. 2.4}$$

2.2.2 Effective Length Factor

It is known that the effective length factor, K is required in computing the compressive strength of columns. The AISC manual recommends either of the two methods for determining the effective length factor- Alternate Design Method or Direct Design Method. Alternate Design Method is a first-order analysis method, and is most commonly used method for determining K. In this method, the Jackson and Moreland monographs are used that are derived from Eq. 2.5 and Eq. 2.6 as specified in the code.

Unbraced Frame:

$$\frac{\gamma_1 \gamma_2 \left(\frac{\pi}{k}\right)^2 - 36}{6\,(\gamma_1 + \gamma_2)} = \frac{\pi/k}{tan(\pi/k)} \qquad \text{Eq. 2.5}$$

Braced Frame:

$$\frac{\gamma_1 \gamma_2}{4}\left(\frac{\pi}{k}\right)^2 + \frac{\gamma_1 + \gamma_2}{2}\left(1 - \frac{\pi/k}{tan(\pi/k)}\right) + \frac{2\,tan(\pi/2k)}{\pi/k} = 1 \qquad \text{Eq. 2.6}$$

Where,

$$\gamma_1 = \sum \frac{I_{c1}/l_{C1}}{I_{b1}/l_{b1}} \; and \; \gamma_2 = \sum \frac{I_{c2}/l_{C2}}{I_{b2}/l_{b2}} \qquad \text{Eq. 2.7}$$

The subscripts c and b refer to the compression and beam elements, respectively, the subscripts 1 and 2 refer to two ends of the compression member under consideration, I is the moment of inertia, and, l is the length of the member under consideration. In Eq. 2.7, the summation sign is for all the connecting elements that restrain from weak-axis buckling, and therefore, the sizes of the connecting beams connecting to the column in the transverse direction must be known. However, since only 2-D planar frames will be considered in this study, the member sizes in the transverse direction are unknown, and therefore this method cannot be considered in this study.

In the AISC Direct Design Method, the code allows the effective length factor to be taken as unity under two conditions- first, the P-Delta second-order effects must be included in the analysis and second, the stiffness of the members must be reduced by 20%, or EI multiplied by a factor of 0.80. So, the forces in the members shall correspond to the reduced stiffness. In addition, a notional load of 0.5% of the vertical loads must be applied at each story, to account for the geometric imperfections [21].

2.3 Review of Current Seismic Design Procedures

2.3.1 Introduction

The conventional philosophy of Building Codes for earthquake-resistant design is to prevent the structures from collapsing in the extreme earthquake event likely to occur at a building site and to limit the structural damage. The Code's approach is to economically design a structure that can withstand a very strong earthquake through sufficient ductility in the structure, and not to design a structure with high strength [22]. Thus, the structures shall have enough ductility to survive strong earthquakes without collapsing. Ductility is the amount of inelastic deformation that the structure can undergo beyond its yield point. Ductility for an earthquake-resistant design is important because it permits the redistribution of internal stresses and forces in the members; results in more robust structures; provides warning of failure, and prevents a structure from collapsing under severe earthquake loads.

There are three main criteria required to develop ductile behavior in earthquake-resistant buildings. First is choosing frame members that must be allowed to yield during earthquakes; for example, beams in moment resisting frames, braces in concentrated braced frames, links in eccentrically braced frames etc. These members are also known as "Deformation-Controlled" or "Fuse" elements, as these are members that have the capability to absorb energy and exhibit highly

inelastic ductile behavior [23]. Secondly, these "fuses" must be provided with sufficient seismic or steel detailing so that they can sustain target ductility or inelastic deformations prior to their failure. The third requirement is to design the "Force-Controlled" elements to be stronger than the fuses or deformation-controlled elements. The force-based elements are typically the members that are critical for the structure's stability, or the members that prevents structural collapse. These typically constitute columns in moment frames, beams in concentrically and eccentrically braced frames, transfer girders, etc. The ultimate objective behind designing fuses and force-controlled elements as per the preceding criteria is to achieve the target yield mechanism of collapse prevention, as described in the capacity design concept below.

2.3.2 Capacity Design Principles

The capacity design method was initially proposed by John Hollings in the year 1968 [24] related to the seismic-resistant design of frame buildings. The concept of capacity design is to ensure a desirable mechanism of inelastic response under seismic attacks, by providing a "strong-column-weak beam" hierarchy [25]. This is achieved by allowing the fuse or deformation-controlled elements to yield by designing them to be weaker than the force-controlled elements; whereas, the force-controlled or protected elements are designed for the maximum (overstrength) force capacity, as can be seen in Eq. 2.8.

$$\phi C_n \geq \gamma D_n \qquad \text{Eq. 2.8}$$

Where,

C_n = Nominal strength of the force-controlled component

D_n = Nominal force demand, imposed by the yielding component

$\phi \; and \; \gamma$ = Demand and capacity factors (similar to load and resistance factors)

There are two approaches in designing the force-controlled elements, i.e., the local approach and the global approach. Eq. 2.8 shows the local approach where the required forces in these elements; for example, columns in moment-frames, are taken as the forces induced by the yielding component such as beams, D_n multiplied by the capacity factor, γ. As an alternative, in the global or simplified approach, the required forces in columns can be taken as the induced forces due to seismic loads multiplied by an empirical overstrength factor, Ω [25]. These are also referred to as the amplified seismic forces.

2.3.3 ASCE 7-10 Equivalent Lateral Force Procedure (EFP)

EFP is a simplified seismic analysis/design procedure codes as an alternative to complex nonlinear or incremental dynamic analysis (IDA) procedures, specified in the ASCE 7-10 codes. This is one of the most commonly used modern seismic design procedure which works generally well with low to mid-rise structures with regular geometric configuration [26]. The design approach relies on the inelastic response/yielding of building elements to control structural damage under large earthquake loads. The method uses empirical seismic performance parameters such as response modification factor, R, displacement amplification factor, C_d, and overstrength factor, Ω_o. The seismic design procedure is for design (Life-Safety) earthquake level with a return period of 475-years. A site-specific design acceleration response spectrum is used to predict the seismic demand or the base shear for a building, where a response spectrum is a plot of the peak response (displacement, velocity, or acceleration) of a series of single-degrees-of-freedom (SDOF) oscillators of varying natural frequency subjected to the same ground motions [22].

The design approach of this method can be explained with the help of Figure 2.2, which is a plot of seismic base shear, V in the y-axis and the story drift, D in the x-axis. In Figure 2.2, the

actual seismic demand or base shear corresponding to the earthquake ground accelerations, are at level E. If a structure was to be designed to remain elastic at level E; there is still no guarantee that the design would be safe, as the earthquakes are highly uncertain and there is a chance that the earthquake forces may exceed level E. It is apparent that it is infeasible to design a structure that relies on its linear response to sustain such large loads. Thus, the code of practice is to reduce the seismic base shear at level E, V_e by the response modification factor, R, which takes the effects of energy-dissipation through damping, R_d, and material overstrength, Ω_o into account. Since these effects are difficult or impractical to quantify, a single empirical factor, R is specified by the codes to obtain the base shear at the design level S, that is, V_s. The intent of the R factor is to simplify the structural design process such that linear elastic analysis can be used for the seismic design. However, during earthquakes, the peak story drifts are at level U at the point of ultimate failure, and not at design base shear level S. Therefore, to predict the actual displacement response of the structure, the code requires us to use the displacement amplification factor, C_d, which amplifies the displacement demand from the design level, S to the ultimate failure level, U.

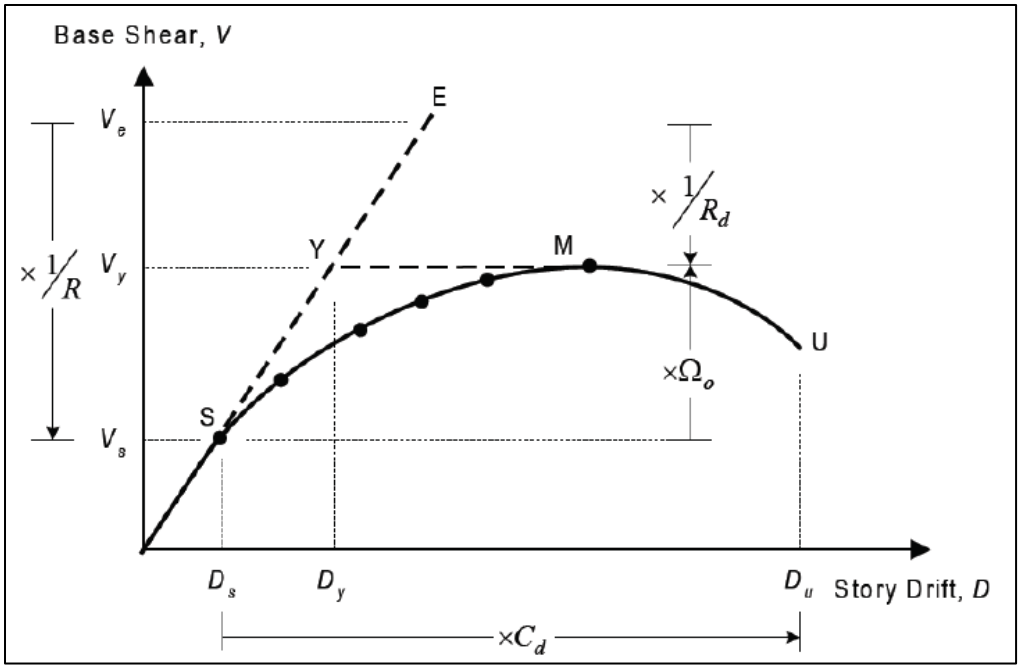

Figure 2.2: Equivalent Static Force Method [22]

To achieve the target yield mechanism of a moment-resisting frame, the strong-column weak-beam hierarchy is enforced as per the capacity design principle discussed above. Therefore, ASCE 7-10 requires deformation-controlled members to be designed for the design level or reduced earthquake forces, at level V_s and then amplifying their displacements responses by the C_d factor. Whereas, the force-controlled members or columns are to be designed for the amplified seismic forces, i.e., design level forces at V_s multiplied by a single overstrength factor, Ω_o.

The ASCE 7-10 EFP seismic design steps can be summarized in the following steps:

1) Fundamental Period, T [27]: The fundamental period of the structure shall be determined either from the substantiated modal analysis or using an approximate fundamental period as per Eq. 2.9. However, if the period is determined from the modal analysis, it shall not exceed the product of the coefficient C_u (Table 2.1) and the approximate fundamental period, T_a.

$$T_a = C_t h_n^x \quad \text{Eq. 2.9}$$

Where, h_n is the structural height in feet, and the coefficients C_t and x are determined from Table 2.2.

Design Spectral Response Acceleration Parameter at 1 s, S_{D1}	Coefficient C_u
≥ 0.4	1.4
0.3	1.4
0.2	1.5
0.15	1.6
≤ 0.1	1.7

Table 2.1: Coefficient for Upper Limit on Period [27]

Structure Type	C_t	x
Moment-resisting frame systems in which the frames resist 100% of the required seismic force and are not enclosed or adjoined by components that are more rigid and will prevent the frames from deflecting where subjected to seismic forces:		
Steel moment-resisting frames	0.028 (0.0724)[a]	0.8
Concrete moment-resisting frames	0.016 (0.0466)[a]	0.9
Steel eccentrically braced frames in accordance with Table 12.2-1 lines B1 or D1	0.03 (0.0731)[a]	0.75
Steel buckling-restrained braced frames	0.03 (0.0731)[a]	0.75
All other structural systems	0.02 (0.0488)[a]	0.75

[a]Metric equivalents are shown in parentheses.

Table 2.2: Values of Approximate Period Parameters C_t and x [27]

2) Design acceleration response spectrum [28]: The ASCE 7-10 code makes use of the mapped seismic acceleration response (at 5% damped) parameters, S_{DS} and S_{D1}, that can be used to obtain the design response spectrum by making use of the following equations, as shown in Figure 2.3.

For $T < T_0$ $\quad S_a = S_{DS}\left(0.4 + 0.6\frac{T}{T_O}\right)$ Eq. 2.9

For $T_0 \leq T \leq T_S$ $\quad S_a = S_{DS}$ Eq. 2.10

For $T_S < T \leq T_L$ $\quad S_a = \frac{S_{D1}}{T}$ Eq. 2.11

For $T > T_L$ $\quad S_a = \frac{S_{D1}T_L}{T^2}$ Eq. 2.12

Where,

S_{DS} = Design spectral response acceleration parameter at short periods

S_{D1} = Design spectral response acceleration parameter at 1-s period

T = Fundamental period of the structure

$T_0 = 0.2\ \frac{S_{D1}}{S_{DS}}$

$T_S = \frac{S_{D1}}{S_{DS}}$

T_L = Mapped long-period transition period (s)

3) Determine the seismic weight of the structure, W, which is basically all the inertial mass that resists seismic forces due to the ground motion. This includes, all the dead load of all permanent components of the building and permanent equipment, 25% of the design storage live load (except in public garages and open parking structures, a uniform load of 10 psf if partition loads are considered, and a portion of the snow load, i.e., 20% of p_f in regions where the flat roof snow load exceeds 30 psf [29].

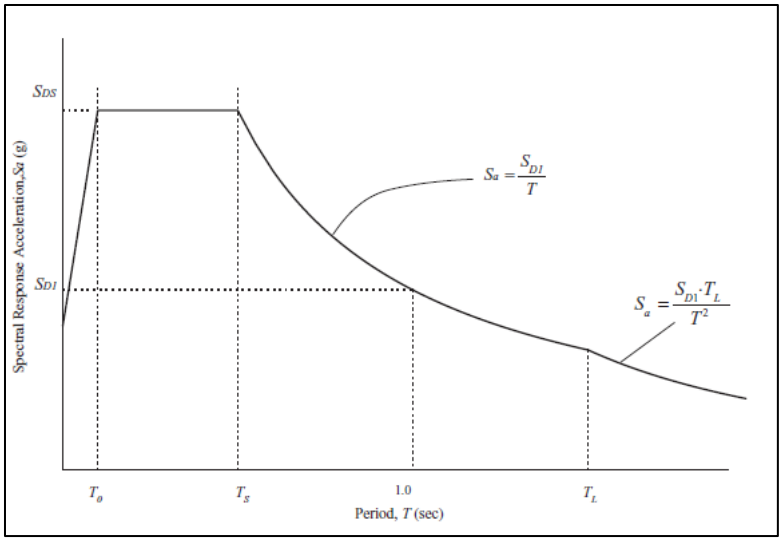

Figure 2.3: Design Response Spectrum [28]

4) Determine Seismic Base Shear [30]: The seismic base shear, V (kips) is given by the following equation:

$$\text{Base Shear, } V = C_S W \qquad \text{Eq. 2.13}$$

Where,

C_S = seismic response coefficient

W = the effective seismic weight

The seismic response coefficient, C_S shall be determined using the following equation, and by complying with its minimum and maximum limits as per the code. Again, this factor reduces the earthquake forces to obtain the design level forces to simplify the analysis to linear elastic and to predict the inelastic response of the structure by making use of the empirical factor, R.

$$C_S = \frac{S_{DS}}{\frac{R}{I_e}} \qquad \text{Eq. 2.14}$$

Where, I_e is the importance factor for earthquakes.

5) Vertical Distribution of Base Shear [31]: For short period buildings, the force distribution generally follows a triangular pattern, i.e., increases linearly along the height of the structure for evenly distributed mass. The lateral force at each level shall be determined in accordance with the following equations.

$$F_x = C_{vx} V \qquad \text{Eq. 2.15}$$

$$C_{vx} = \frac{w_x h_x^k}{\sum_{i=1}^{n} w_i h_i^k} \qquad \text{Eq. 2.16}$$

Where,

C_{vx}	=	Vertical distribution factor
V	=	Total design base shear at the base of structure (kips)
$w_x \; and \; w_i$	=	The seismic weight of story i or x
$h_i \; and \; h_x$	=	The height from the base to the level i or x
k	=	An exponent related to the structure period as follows: For structures having a period of 0.5 s or less, $k = 1$ For structures having a period of 2.5 s or more, $k = 2$ For structures having a period between 0.5 s and 2.5 s, k shall be interpolated between 1 and 2.

6) To meet the capacity design requirement, ASCE 7-10 provides two LRFD load case combinations for earthquake loads [32]: basic load combination for deformation-controlled elements (beams) and load combination with overstrength factor for force-controlled elements (columns) as follows:

Beams:

$$\text{LCC 5: } (1.2 + 0.2S_{DS})D + 1.0E + L + 0.2S \qquad \text{Eq. 2.17a}$$

$$\text{LCC 7: } (0.9 - 0.2S_{DS})D + 1.0E \qquad \text{Eq. 2.17b}$$

Columns:

$$\text{LCC 5: } (1.2 + 0.2S_{DS})D + \Omega_o E + L + 0.2S \qquad \text{Eq. 2.18a}$$

$$\text{LCC 7: } (0.9 - 0.2S_{DS})D + \Omega_o E \qquad \text{Eq. 2.18b}$$

7) Design Story Drifts [33]: The design deflections shall be obtained as per the following equation and shall not exceed the allowable story drift limits given in Table 2.3.

$$\delta_x = \frac{C_d \delta_{xe}}{I_e} \qquad \text{Eq. 2.19}$$

Where,

C_d = Deflection amplification factor from ASCE 7-10, Table 12.2-1

δ_{xe} = Deflection determined by an elastic analysis

I_e = Importance factor determined in ASCE 7-10, Section 11.5.1

The design story drift, Δ shall be computed as the difference of the deflections at the top and bottom of the story under consideration, as shown in Figure 2.4.

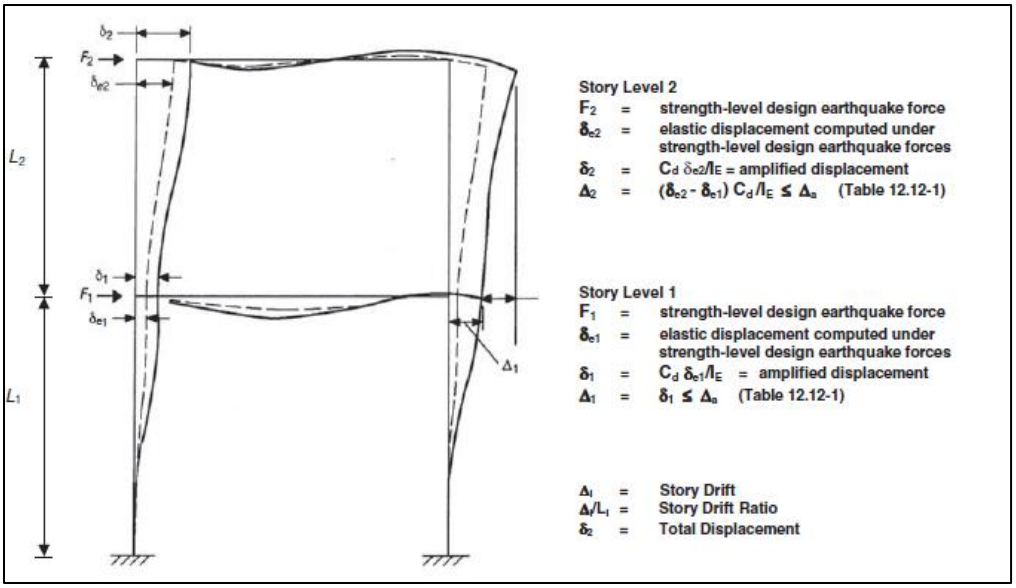

Figure 2.4: Story Drift Determination [33]

Structure	Risk Category		
	I or II	III	IV
Structures, other than masonry shear wall structures, 4 stories or less above the base as defined in Section 11.2, with interior walls, partitions, ceilings, and exterior wall systems that have been designed to accommodate the story drifts.	$0.025h_{sx}$[c]	$0.020h_{sx}$	$0.015h_{sx}$
Masonry cantilever shear wall structures[d]	$0.010h_{sx}$	$0.010h_{sx}$	$0.010h_{sx}$
Other masonry shear wall structures	$0.007h_{sx}$	$0.007h_{sx}$	$0.007h_{sx}$
All other structures	$0.020h_{sx}$	$0.015h_{sx}$	$0.010h_{sx}$

[a] h_{sx} is the story height below Level x.
[b] For seismic force-resisting systems comprised solely of moment frames in Seismic Design Categories D, E, and F, the allowable story drift shall comply with the requirements of Section 12.12.1.1.
[c] There shall be no drift limit for single-story structures with interior walls, partitions, ceilings, and exterior wall systems that have been designed to accommodate the story drifts. The structure separation requirement of Section 12.12.3 is not waived.
[d] Structures in which the basic structural system consists of masonry shear walls designed as vertical elements cantilevered from their base or foundation support which are so constructed that moment transfer between shear walls (coupling) is negligible.

Table 2.3: Allowable Story Drift Limits [34]

It shall be noted that the code permits to determine the elastic drifts, δ_e using the seismic design forces based on the computed fundamental period of the structure instead of the upper limit period ($C_u T_a$) specified in step 1 [33].

2.3.4 ASCE 7-10 Linear Response Time-History Analysis

Both 2-D and 3-D analysis are permitted for the response history procedures. A linear model of the structure shall be used in determining its response through the methods of numerical integration. A suite of ground motion acceleration records compatible with the design response spectrum shall be used for the considered location of the structure. A suite of no less than three appropriate ground motions shall be used in the analysis [35]. Each ground motion must consist of a horizontal acceleration history selected from an actual recorded earthquake event [35]. Additionally, the ground motions can be simulated that are compatible with the design response spectrum, to make up the total number required. These ground motions shall be scaled such that the average value of the 5 percent damped response spectra for the suite of motions considered is not less than the design response spectrum for the site between the periods $0.2\ T\ and\ 1.5\ T$, where T is the natural period of the structure in the fundamental mode for the direction of response being analyzed [35]. For determining the displacement or force response of the structure, the following scaling parameters must be used:

a. Force quantities shall be multiplied by the factor I_e/R, where I_e is the importance factor and R is the response modification factor as discussed in the previous sections [35].
b. The story drifts shall be multiplied by C_d/R, where C_d is the displacement amplification factor specified in Table 12.2-1 of the code. The allowable story drift limits are permitted to be taken as 125% of the limits specified in Table 2.3. [35].

Where the maximum scaled (as above) base shear obtained from this analysis procedure (V_i) is less than the 85% of the minimum base shear obtained in the equivalent lateral force procedure and where the acceleration response parameter S_1 is equal to or greater than 0.6g; then, the scaled member forces shall be multiplied by $\frac{V}{V_i}$, where V is the minimum base shear [36].

Additionally, if the maximum scaled base shear predicted in this analysis or V_i is less than $0.85C_sW$, where C_s is the upper limit of the response modification factor given in ASCE 7-10, Eq. 12.8-6.; then drifts shall be multiplied by $0.85\ C_sW/V_i$ [36].

Lastly, if a suite of at least seven ground motions are considered in the analysis, then the design member forces and drifts shall be taken as the average of the forces and drifts determined from the analyses of the suite and as scaled in the preceding text [36]. If fewer than seven ground motions are analyzed, then the design member forces and the design drifts shall be taken as the maximum of the scaled force and scaled drift quantities determined from analyses [36]. Where, the overstrength factor is used in the load combinations, then the value of the amplified force responses need not be taken larger than the maximum of the unscaled force response obtained from the analyses [36].

2.3.5 Nonlinear Static Procedures

The nonlinear static procedure (NSP), also known as pushover analysis, is a simplified method that has a capacity to adequately predict the nonlinear behavior of a structure under seismic loads and estimate the strength capacity beyond the elastic limits, as an alternative to performing rigorous IDA (incremental dynamic analysis) procedures. The use of pushover analysis has accelerated in the United States since the publication of ATC-40, FEMA 274, and FEMA 356 documents [37]. It is a popular tool for the estimation of seismic demands and for the performance evaluation of new and existing structures under different seismic hazard levels. The pushover analysis is a static nonlinear analysis of a structure under permanent gravity loads and monotonically increasing lateral loads. The analysis can be carried up to failure of the structure, thus it helps in the determination of nonlinear characteristics of a structure such as post-yield

stiffness, ductility, and ultimate failure strength. The result is a plot between the base shear of the structure and the roof or top displacement.

There are three main nonlinear static analysis provisions in the current U.S. code of practice including: ATC-40 Capacity Spectrum Method (CSM), FEMA 274 Coefficient Method, and FEMA 356 Coefficient Method (CM) [37]. The main difference between capacity spectrum method and coefficient method is that CSM obtains the performance point or seismic demand by converting a nonlinear SDOF system into an equivalent linear SDOF system with an assumption that, for a SDOF system, inelastic displacement will be approximately equal to the elastic displacement with greater period and damping values than the initial values in nonlinear system [38]. Whereas, CM obtains the maximum displacement of the MDOF system, termed as target displacement, by modifying the linear elastic response of the equivalent SDOF system by multiplying it by a series of coefficients obtained from empirical equations derived by calibration for a large number of dynamic analyses [38]. In this study, the Coefficient Method of FEMA 356 will be used because of the following reasons:

a. It has been adopted in the ASCE-41 provisions [39].
b. It has shown to provide more accurate results as compared to ATC CSM procedure [40].
c. ATC-40 CSM tends to overestimate the demand under Maximum Considered Earthquake (MCE), resulting in higher costs [40].

2.3.6 FEMA 356 Coefficient Method

The analysis procedure is based on a nonlinear mathematical model of a structure that directly incorporates the nonlinear load-deformation relation of all the structural components and elements, and the structure shall be subjected to monotonically increasing lateral loads under permanent gravity loads, until the target displacement point exceeded [41]. These loads represent the inertial

forces experienced during an earthquake. The analysis steps are summarized in the form of following requirements as per FEMA 356:

1) Modeling Considerations [41]: By performing the pushover analysis in combination with the gravity loads, the relation between the base shear and lateral displacement of the control node shall be established. The control node shall be located at the center of mass of the roof. The nonlinear behavior of all the components shall be included in the model that uses full backbone curve and includes strength degradation and residual strength, if any. At least two lateral load distributions shall be considered in the analysis. When more than 75% of the total mass participation is from the fundamental mode in the direction under consideration, this distribution is permitted to be either proportional to the C_{vx} coefficients found from Eq. 2.16 or proportional to the fundamental mode in the direction under consideration. The second lateral load distribution pattern shall be proportional to the total mass at each level.

2) Bilinear Idealization [42]: The next step in the procedure is to replace the obtained pushover curve or the plot of the base shear and the nonlinear deformation of the control node with an idealized bilinear curve. The idealized relationship is used to calculate the effective lateral stiffness, K_e, and effective yield strength, V_y of the building as shown in Figure 2.5. The two line segments shall be located such that area under the curve and above the curve are approximately equal. This is done by using an iterative procedure in which the slopes of the two lines segments are changed until the areas above and below the curve are approximately balanced. The point where the two lines meets is taken as the effective yield strength, V_y, and then effective lateral stiffness, K_e is taken as the secant slope calculated at the base shear equal to the 60% of the effective yield strength of the structure.

The post-yield slope, α, is the ratio of the post-yield stiffness (slope of the second line segment) and effective lateral stiffness, K_e. Next, an effective fundamental period in the direction under consideration shall be determined using the initial elastic lateral stiffness (slope of the actual curve in the elastic region), K_i, effective lateral stiffness, K_e, and initial fundamental time period calculated in elastic modal/dynamic analysis, T_i:

$$T_e = T_i \sqrt{\frac{K_i}{K_e}} \qquad \text{Eq. 2.20}$$

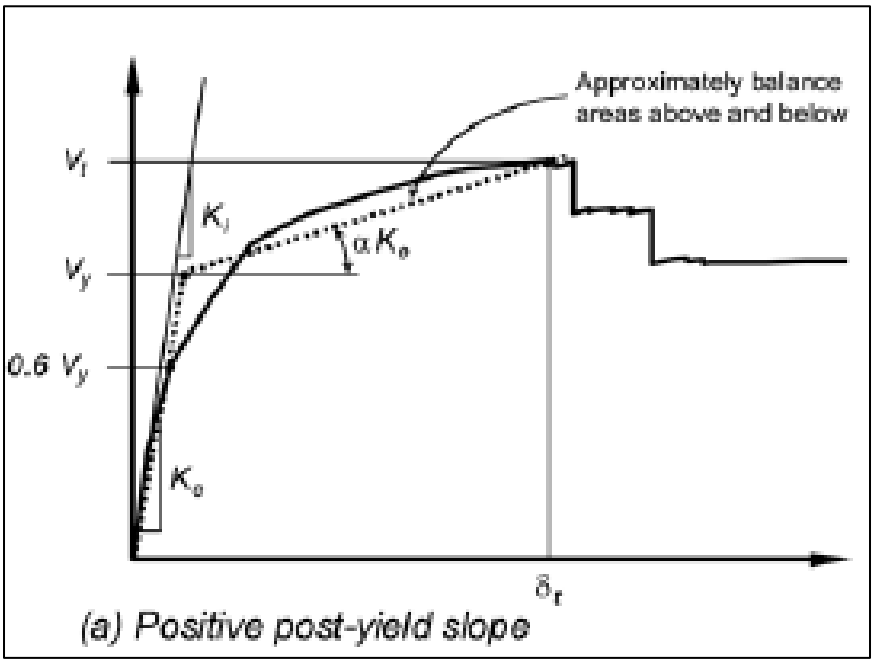

Figure 2.5: Idealized Force-Displacement Curves [43]

3) Target Displacement [43]: The target displacement is intended to represent the maximum displacement that is likely to occur during the design earthquake, and the calculated internal forces and stresses at this level are reasonable approximations of those expected during the design earthquake because the model takes the nonlinear response of the

structure into account. The target displacement, δ_t shall be calculated as per the following equation:

$$\delta_t = C_0\, C_1\, C_2\, C_3\, S_a\, \frac{{T_e}^2}{4\pi^2}\, g \qquad \text{Eq. 2.21}$$

Where:

$C_0 =$ Modification factor that relates spectral displacement of an equivalent SDOF system to the roof displacement of the building MDOF system, taken from Table 2.4.

$C_1 =$ Modification factor to relate expected inelastic displacement to linear elastic response.

$= 1.0$ for $T_e \geq T_s$

$= [1.0 + (R - 1)T_s/T_e]/R$ for $T_e < T_s$

but shall not be greater than 1.5 and less than 1.0 as per FEMA 356, Section 3.3.1.3.

$R =$ Ratio of elastic seismic demand to yield strength coefficient given as follows:

$$R = \frac{S_a}{V_y/W}.C_m \qquad \text{Eq. 2.22}$$

Where:

$V_y =$ Yield strength calculated as before

$W =$ Effective seismic weight of the building

$C_m =$ Effective mass factor for the fundamental mode taken from Table 2.4 or using Eigenvalue analysis.

$C_2 =$ Modification factor to represent the effect of pinched hysteretic shape, stiffness degradation, and strength deterioration. $C_2 = 1.0$ is permitted for nonlinear procedures.

$C_3 =$ Modification factor to represent increased displacements due to dynamic P-Δ effects.

For buildings with post-yield stiffness, C_3 can be taken as 1.0.

S_a = Response spectrum acceleration, at the effective fundamental period and damping ratio of the building in the direction under consideration [44].

g = Acceleration due to gravity.

Table 3-1 Values for Effective Mass Factor C_m[1]

No. of Stories	Concrete Moment Frame	Concrete Shear Wall	Concrete Pier-Spandrel	Steel Moment Frame	Steel Concentric Braced Frame	Steel Eccentric Braced Frame	Other
1–2	1.0	1.0	1.0	1.0	1.0	1.0	1.0
3 or more	0.9	0.8	0.8	0.9	0.9	0.9	1.0

1. C_m shall be taken as 1.0 if the fundamental period, T, is greater than 1.0 second.

Table 2.4: Effective Mass Factor [45]

4) Acceptance Criteria [46]: The forces and deformations corresponding to the control node displacement equaling or exceeding the target displacement forms the seismic demand or the required forces and deformations for the design. Therefore, the capacities of the structural components shall not be less than the maximum deformation demands calculated at the target displacement. For the primary and secondary steel components of the structure, the nonlinear modeling criteria, strength and deformation capacities, and their acceptance criteria are provided in Chapter 5 of the FEMA 356 document. Since, an OpenSees nonlinear mode will be used in this study (see Ch. 5.4), the code's modeling criteria will not be covered. The acceptance criteria for the primary components, beams and columns are given as follows:

   a. Beams: Flexural actions shall be considered as deformation-controlled elements, and shall conform to permissible plastic rotations as indicated in FEMA 356, Table 5-6. But, in this paper, the plastic rotation limits specified in the AISC Seismic Provisions [47] will be used. (Appendix B).

b. Columns: For steel columns under combined axial and bending forces, where the column axial load is less than 50% of the lower bound column strength, P_{CL}, the column shall be considered as deformation-controlled element and shall comply with the maximum permissible plastic rotations specified in the code (Appendix B). Where the axial compressive load exceeds 50% of the lower-bound column strength, P_{CL}, the column shall be considered as force-controlled element for both axial loads and flexural loads, and shall conform to the following equation:

$$\frac{P_{UF}}{P_{CL}} + \frac{M_{F,x}}{M_{CL,x}} + \frac{M_{F,y}}{M_{CL,y}} \leq 1 \qquad \text{Eq. 2.23}$$

Where:

x, y = Member's forces/strengths about the x-axis and y-axis.

P_{UF} = Required axial force in the member.

M_{UF} = Required bending moment in the member about the x-axis.

P_{CL} = Lower-bound axial compression strength (Appendix C) Seismic Provisions, taking strength reduction factor, $\phi = 1.0$ and using lower-bound value for yield strength (Appendix C)

M_{CL} = Lower-bound flexural strength determined as per AISC *Seismic Provisions*, taking strength reduction factor, $\phi = 1.0$ and using lower-bound value for yield strength (Appendix C).

2.3.7 Performance-Based Design

Traditionally, the seismic design of structures has been strength-based and met the minimum safety requirements of the occupants. However, recent earthquakes like Northridge (1994) and Kobe (1995) showed that buildings experienced significant damages even when their

designs were compliant with the code [48]. This resulted in closure of critical facilities including schools, hospitals, etc., and interruption of businesses, even if the structural damages were minor. Thus, designs that meet the minimum code criteria are not sufficient. In light of this, it was recognized that designs that meet the performance objective of the community's stakeholders, while meeting the minimum safety design criteria at the same time needs to be developed. This led to the development of a performance-based design methodology, as an enhanced design requirement in addition to the current strength-based methods.

The growing acceptability of the performance-based design approach is evident in the studies related to the seismic rehabilitation of existing buildings, published by FEMA, ATC, and SEAOC [49]. The concepts and guidelines for seismic rehabilitations can also be used for new buildings in the form of performance-based design [49]. In this paper, the performance-based design will be in accordance with FEMA 356, which is a joint work of FEMA and ASCE.

The code recognizes four building performance-levels as objectives namely, Operational Performance (OP), Immediate Occupancy (IO), Life Safety (LS), and Collapse Prevention (CP). These objectives are used in conjunction with the probabilistic seismic hazard levels, to select target goals considering basic, enhanced, or limited objectives as defined below.

		Target Building Performance Levels			
		Operational Performance Level	**Immediate Occupancy Performance Level**	**Life Safety Performance Level**	**Collapse Prevention Performance Level**
Earthquake Hazard Level	50%/50 year	a	b	c	d
	20%/50 year	e	f	g	h
	BSE-1 (10%/50 year)	i	j	k	l
	BSE-2 (2%/50 year)	m	n	o	p

Table 2.5: Rehabilitation Objectives [50]

The code defines the above objectives based on the above table as follows:

k + p	=	Basic Safety Objective (BSO)
k + p + any of a, e, i, b, f, j, or n	=	Enhanced Objectives
o alone or n alone or m alone	=	Enhanced Objectives
k alone or p alone	=	Limited Objectives
c, g, d, g, l	=	Limited Objectives

Thus, the above definitions of limited, basic safety, and enhanced objectives can be useful in selecting the seismic hazard levels for the performance-based design of buildings. The figure below taken from FEMA 274 illustrates the costs associated with the above performance objectives in conjunction with the earthquake hazard levels.

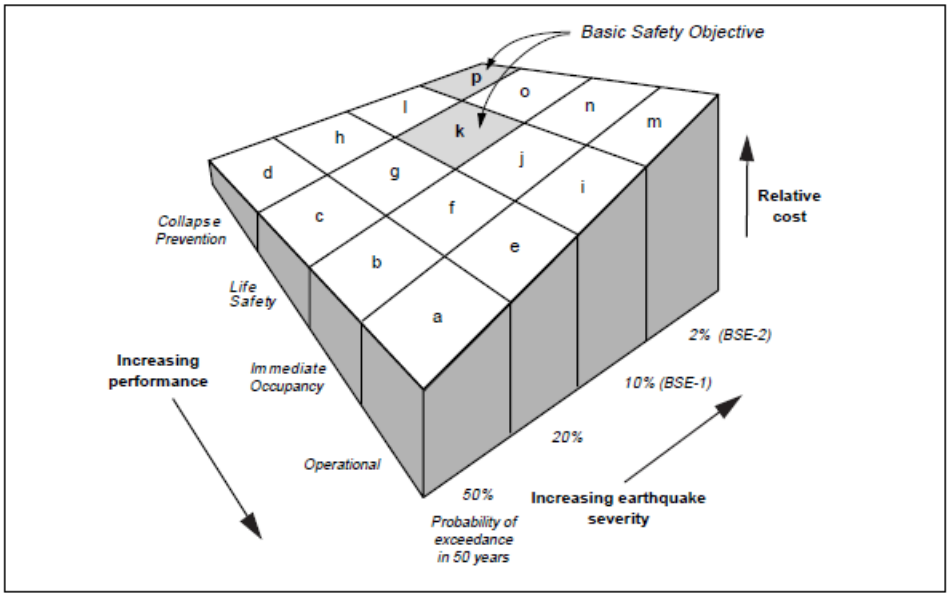

Figure 2.6: Surface showing Relative Costs of Various Rehabilitation Objectives [51]

For different target building performance levels of Immediate Occupancy, Life Safety, and Collapse Prevention, the definition of structural and nonstructural performance criteria corresponding to these target performance levels have been specified in the code. For the performance-based design of steel moment frames, the drift limits for target performance levels are specified in the code as follows:

Structural Performance Level	Drift Ratio (%)
Immediate Occupancy	0.7%
Life Safety	2.5%
Collapse Prevention	5%

Table 2.6: Drift limits for different target performance levels [52]

Chapter 3: PSO Validation

3.1 Introduction

Recently many studies have been undertaken to improve the performance of the original PSO algorithm, such as particle swarm optimizer with passive congregation (PSOPC), harmony search (HS) scheme, heuristic particle swam optimizer (HPSO), etc. [4]. However, it shall be noted that their performance depends on the problem and selection of algorithm parameters, and each have different limitations. In this study, the two main algorithms considered are the standard PSO and the HPSO algorithms depending on the structure type and analysis case.

The main difference between the PSO and HPSO algorithms lies in their constraints-handling technique. The HPSO uses a technique known as 'fly-back mechanism' introduced by He et al. [53]. Since for most of the constrained optimization problems, the optimal solution is located close the constraints boundary or feasible region, the particles in this technique are initialized in the feasible region [54]. When the optimization process starts, the particles fly in the feasible space to search the optimal solution; and if any one of the particles flies outside the feasible boundary, it is forced to fly back to the previous position, and the particle in the next iteration will be closer to the feasible boundary. In this way, the probability of finding a global minimum becomes very high if it is near the boundary [54]. Also, experiments have shown that the 'fly-back mechanism' can help find a better solution with fewer iterations than the other techniques.

In this section, a HPSO code developed in MATLAB is validated by comparing the optimization results obtained in MATLAB to the previously obtained results [54, 55]. Two structures will be used as examples for this purpose. First is a 10-bar planar truss structure [54], and the second example is a six-story two-bay rigid steel frame [55]. For these two structures, the

HPSO algorithm presented by Li, L.J. and Huang, Z.B. [54] will be used given their proven higher convergence rate and better search results. The objective of this step is to validate the HPSO algorithm, so that the optimization code is fit for the proceeding studies of this thesis.

3.2 Code Development

A basic representation of the HPSO code developed in MATLAB for the optimization of steel structures is illustrated in Figure 3.2. The HPSO algorithm is applied to a 10-bar planar truss structure and a six-story steel frame. The strength and serviceability of the design are in accordance with the AISC steel manual. The set of design variables (the positions of the particles within the swarm) can be continuous or discrete as discussed in Chapter 2. In the 10-bar truss structure, the cross-section areas of the truss members are taken as continuous design variables; whereas for the six-story steel rigid frame, a set of a total of 273 AISC W-shapes are selected as discrete design variables. The structural analysis was done in MATLAB using a numerical finite-element analysis method which involved generating local element stiffness matrices, a global structure stiffness matrix, and nodal/equivalent load force matrix. The displacement matrix was determined using equilibrium equations in order to obtain nodal displacements, strains, stresses, and member forces.

3.2.1 10-bar Planar Truss

The 10-bar planar truss geometry with four concentrated loads is shown in Figure 3.1. The material density and the modulus of elasticity are given to be as 0.1 lb/in^3 and 10,000 ksi, respectively. In this example, two load cases will be considered: Case 1, $P_1 = 100\ kips,\ P_2 = 0$; and Case 2, $P_1 = 150\ kips,\ P_2 = 50\ kips$. The objective is to obtain the optimal cross-sectional areas of the members using HPSO to minimize the weight of the structure.

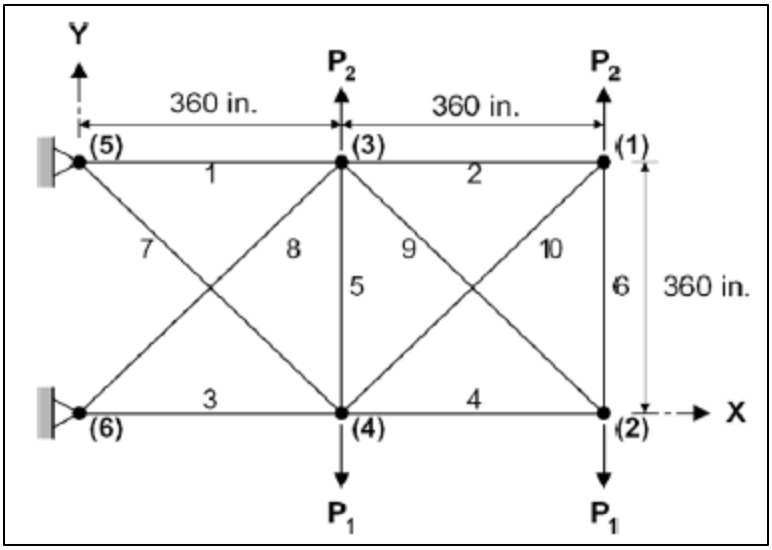

Figure 3.1: 10-bar Planar Truss Structure [54]

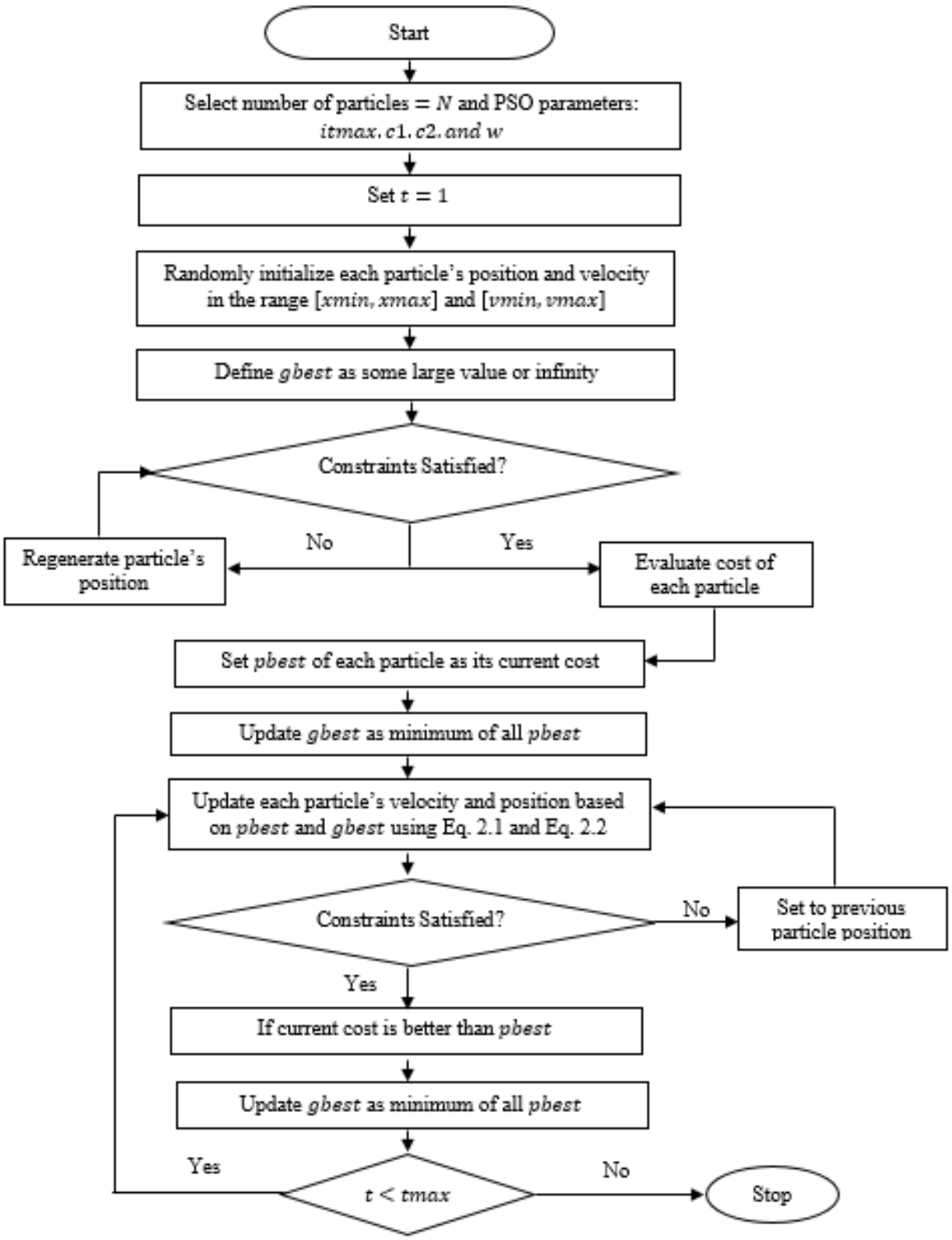

Figure 3.2: HPSO Pseudo Code Flow-Chart

The design constraints and the PSO parameters used in the paper for this structure is summarized in Table 3.1. The minimum permitted cross-sectional area of the 10 design variables or members is 0.1 in.^{2}, the maximum limit can be any large number. In this study, the maximum limit for the design variables was chosen as 100 in.^{2}. The design constraints include maximum tensile/compressive stress of 25 ksi, and maximum nodal displacement limit of ± 2 in. in both horizontal and vertical directions. The same PSO parameters used in the MATLAB code as provided in the paper so that the results are comparable.

Thus, the optimization problem is defined as:

Minimize: $$W = \sum_{k=1}^{m} \rho\, A^k l^k \quad \text{Eq. 3.1}$$

Subject to: $$0.1 < A^k < \infty \quad \text{Eq. 3.2}$$

$$-2 < \delta_j < 2 \quad \text{Eq. 3.3}$$

$$-25 < \sigma < 25 \quad \text{Eq. 3.4}$$

Where: ρ = Material density

l^k = Length of k^{th} member

A^k = Area of k^{th} member

m = Total number of members

δ_j = Displacement of node j

σ = Member stress

Problem Constraints		**PSO Parameters**	
Minimum Cross Sectional Area	0.1 $in.^2$	No. of particles	50
Stress Limits	$\pm$ 25 ksi	Max. Iterations	3000
Nodal Displacement Limits	$\pm$ 2 $in.$	w	Linearly varies from 0.9 to 0.4
-	-	c_1 and c_2	2

Table 3.1: Numerical Example 1: Problem constraints and PSO parameters

The optimization was performed and the obtained results were compared with the ones provided by L.J. Li et al. [54]. Figures 3.3 and 3.4 shows the HPSO convergence comparison for the 10-bar truss structure for Case 1, and Figures 3.5 and 3.6 shows the same for Case 2. The comparison of optimal designs for the 10-bar truss structure for Case 1 and Case 2 are shown in Table 3.2 and Table 3.3, respectively. These tables show the comparison of the optimal cross sectional areas of the members and the optimal weight of the 10- bar truss structure obtained in MATLAB using the developed HPSO code with the results provided in the paper. The HPSO optimal weight of the truss obtained in MATLAB for Case 1 is 5063.3 lb. and for Case 2 is 4682.3. It can be seen that both the convergence rate and the optimal cross-sectional areas, obtained in MATLAB are very similar to the ones given in the paper, within 0.1% of difference.

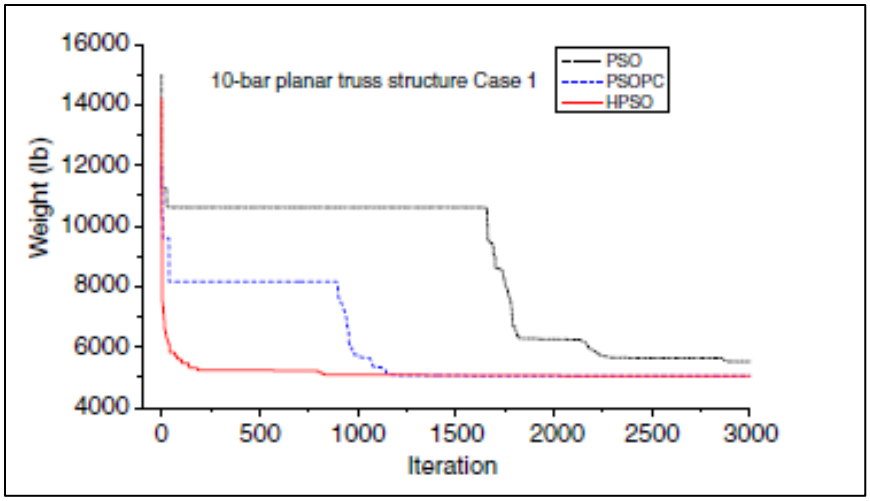

Figure 3.3: Comparison of the convergence rates for the 10-barp planar truss structure (Case 1) by L.J. Li et al. [54]

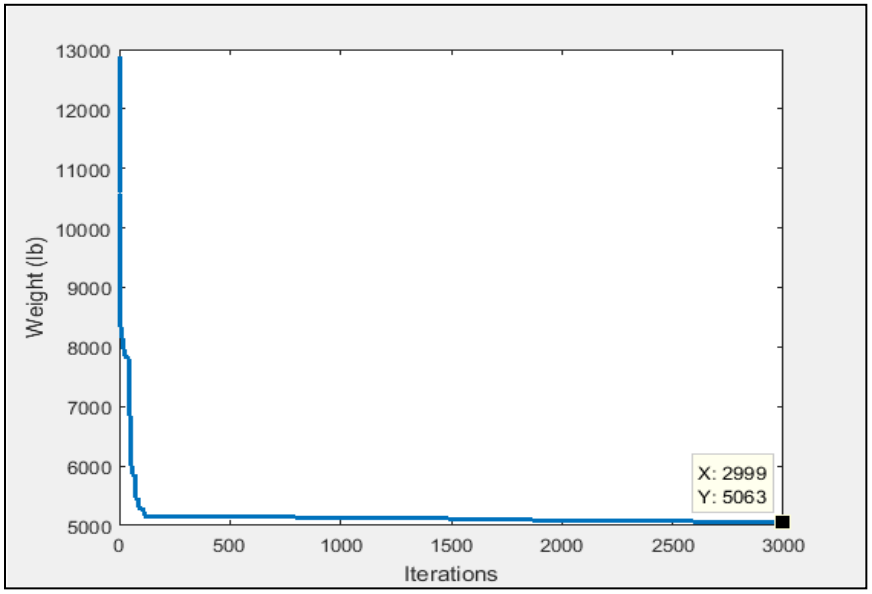

Figure 3.4: MATLAB result for the 10-bar planar truss structure (Case 1)

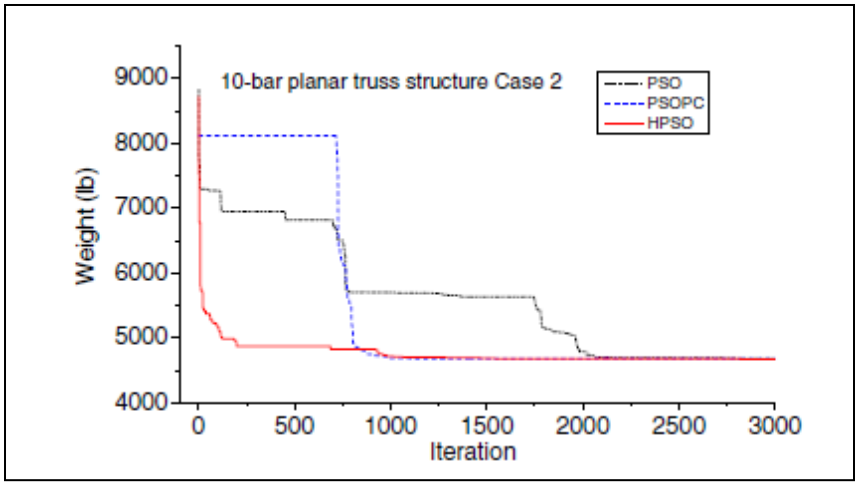

Figure 3.5: Comparison of the convergence rates for the 10-barp planar truss structure (Case 2) by L.J. Li et al. [54]

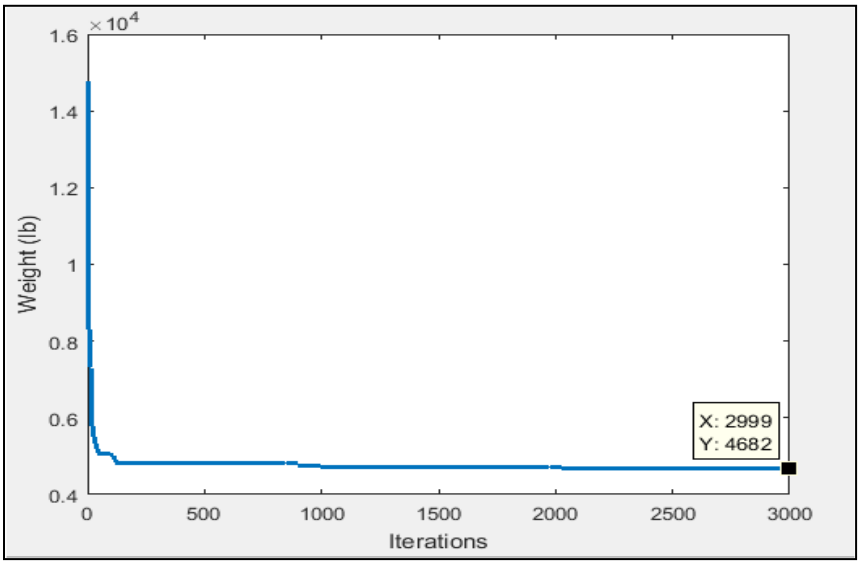

Figure 3.6: MATLAB HPSO graph for the 10-bar planar truss structure (Case 2)

Variables	Area (in.^{2})	HPSO Optimum Areas Comparison	
		L.J. Li et al. [54]	HPSO
1	A_1	30.704	30.9401
2	A_2	0.1	0.1102
3	A_3	23.167	23.2006
4	A_4	15.183	15.3488
5	A_5	0.1	0.1000
6	A_6	0.551	0.5405
7	A_7	7.46	7.4695
8	A_8	20.978	20.8628
9	A_9	21.508	21.3547
10	A_{10}	0.1	0.1002
Weight (lb.)		5060.92	5063.4001

Table 3.2: HPSO MATLAB results comparison for 10-bar planar truss structure (Case 1)

Variables	Area (in.^{2})	HPSO Optimum Areas Comparison	
		L.J. Li et al. [54]	HPSO
1	A_1	23.353	23.348
2	A_2	0.1	0.1
3	A_3	25.502	25.095
4	A_4	14.25	14.234
5	A_5	0.1	0.1
6	A_6	1.972	1.9803
7	A_7	12.363	12.575
8	A_8	12.894	13.199
9	A_9	20.356	20.23
10	A_{10}	0.101	0.1033
Weight (lb.)		4677.3	4682.3

Table 3.3: HPSO MATLAB results comparison for 10-bar planar truss structure (Case 2)

3.2.2 Six-story Steel Rigid Frame

The second structure is a two-bay, six-story steel frame design by E. Doğan and M.P. Saka [55], as shown in Figure 3.7. It is an unbraced frame that consists of thirty members that are divided into eight groups, which forms the discrete design variables for the optimization. The frame is subjected to a uniformly distributed gravity load of $50\ kN/m$ on all floors, and lateral point loads of $25\ kN$ at each story. The allowable problem constraints as provided in the paper are given in Table 3.4.

The beams and columns of the steel frame were designed for axial loading, strong-axis bending, and combined axial and bending effects, in accordance with Chapters D, F, and H of the AISC manual, respectively. The effective length factor, K, used in the design of columns were determined as per the sidesway frame equation C-A-7-2 of the AISC manual.

E. Doğan and M.P. Saka [55] performed optimization for PSO and HS algorithms. In this study, the optimization was performed using HPSO algorithm developed for the previous example. Figure 3.8 shows the PSO graph obtained in the paper and Figure 3.9 shows the HPSO graph obtained in MATLAB. Table 3.8 shows the comparison for the optimal designs with the ones shown in Table 3.5. This is a good example of the statement earlier that the performance of different algorithms are problem-dependent- in the 10-bar truss example, L.J. Li et al. [54] obtained higher optimal cost with PSO than with HPSO (see Tables 3.2 and 3.3); whereas in this example, E. Doğan and M.P. Saka [55] obtained better optimal cost with PSO than with HPSO (see Table 3.5).

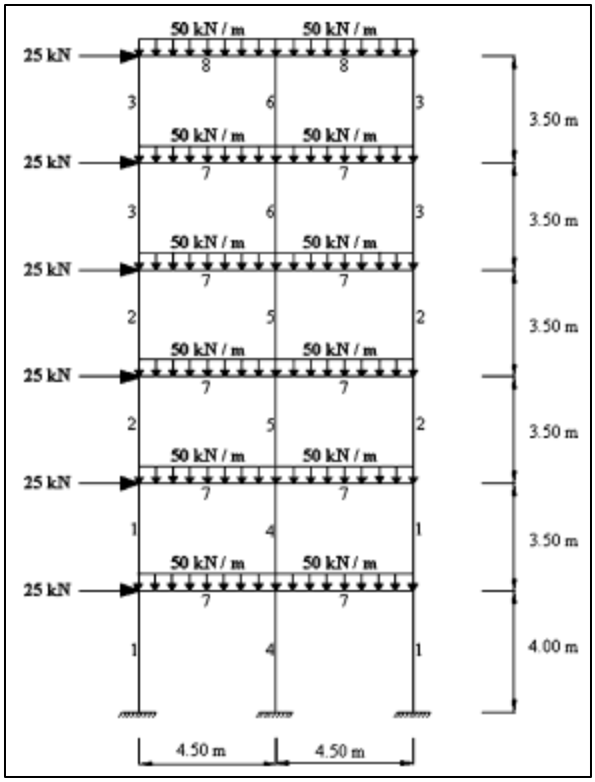

Figure 3.7: Six-story, two-bay rigid steel frame [55]

Problem Constraints		**PSO Parameters**	
Variables	273 AISC W-shapes	No. of particles	40
Max. Roof Displacement	7.17 cm	Max. Iterations	7000
Max. Inter-Story Displacement	1.17 cm	w, c_1, c_2	0.08,2,2

Table 3.4: Numerical Example 2: Problem constraints and PSO parameters

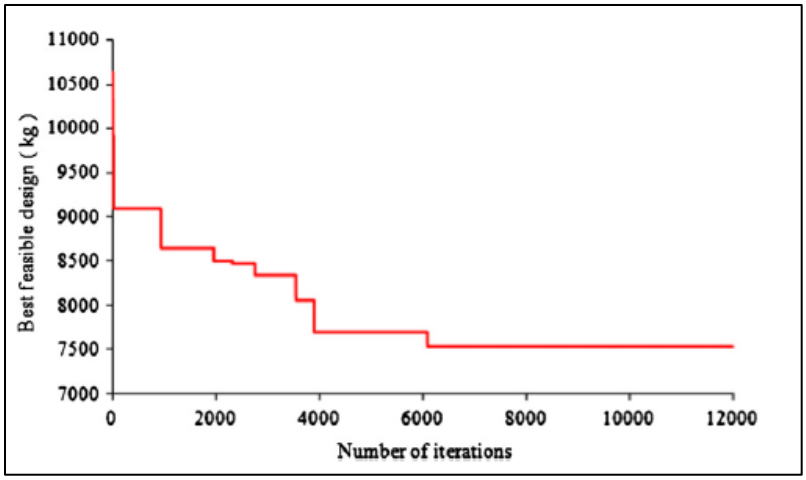

Figure 3.8: PSO graph for six-story, two-bay rigid steel frame by E. Doğan and M.P. Saka [55]

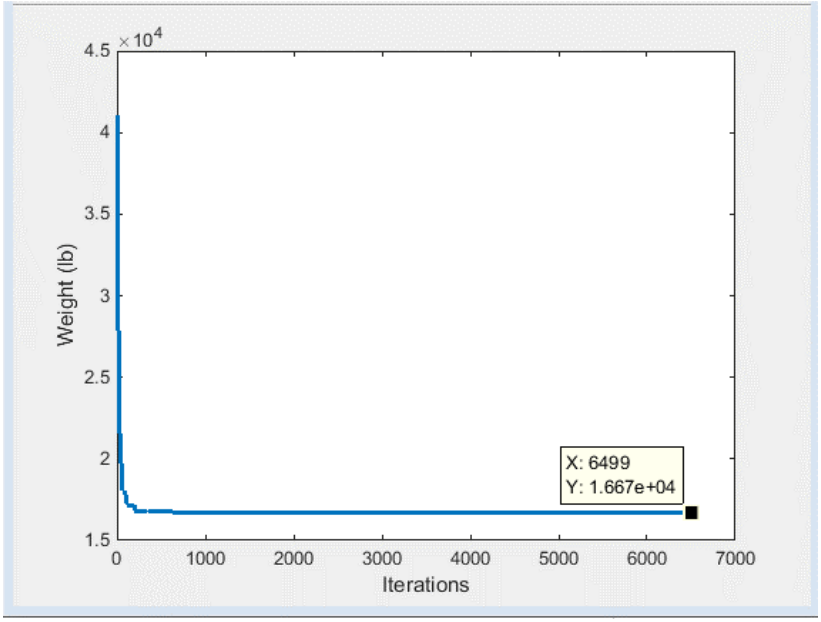

Figure 3.9: MATLAB HPSO graph for six-story, two-bay rigid steel frame

Group No.	Member Type	E. Doğan and M.P. Saka [55]		-
		PSO	HS	HPSO
1	Column	W16X57	W18X55	W12X45
2	Column	W16X40	W12X50	W21X48
3	Column	W10X39	W8X31	W10X22
4	Column	W24X62	W21X73	W27X84
5	Column	W24X62	W18X65	W10X39
6	Column	W8X40	W12X40	W21X44
7	Beam	W14X30	W16X40	W21X44
8	Beam	W18X65	W14X22	W10X60
Minimum Weight (kg)		7533	7829	7561

Table 3.5: HPSO MATLAB results comparison for six-story, two-bay rigid steel frame

.The HPSO graph shown in Figure 3.8 shows the optimal weight as 16670 lb. or 7561 kg. From the comparison of Figures 3.7 and 3.8, it is observed that HPSO has a lot quicker convergence rate than PSO, and their optimal weights are quite close with a difference of 0.1%. The difference in the design member sizes is expected because of the following reasons:

1) There is no unique solution in this optimization problem, as multiple design combinations are possible that results in an optimal solution.
2) The assumptions undertaken during the analysis and design procedures in the paper are unknown.
3) E. Doğan and M.P. Saka [55] considered additional constraints including shear strength checks, geometric limits such that the flange widths of beams are less than the flange widths of the columns the beams are connected to; and that the depth and weight of the columns in the stories below are more than or equal to the ones in the stories above. However, this study does not include these additional constraints for simplicity, as these are unlikely to govern the final design; and therefore, are not the focus of this study.

From the above two examples, it can be concluded that the developed HPSO algorithm is valid, is capable of producing near optimal results, and is fit for the proceeding applications of this study.

Chapter 4: Benchmark Building: 3-Story Moment Resisting Frame

4.1 Introduction

For the seismic design and performance-based design optimization, a three-story steel moment resisting frame (MRF) is selected [56]. As shown in Figure 4.1, the three-story steel MRF structure is 120 ft. by 180 ft. in plan with six bays in the east-west (E-W) direction (longer side) and 4 bays in the north-south (N-S) direction (shorter side) with equal bay widths of 30ft. on center in both directions. The lateral load-resisting system of the building is comprised of steel perimeter MRFs with simple framing between the two furthest E-W frames. The interior bays of the structure are comprised of simple framing with composite floors as shown in the plan (Figure 4.2).

The columns of the building are wide-flange 50 ksi steel and the levels of the 3-story building are numbered with respect to the ground level, as shown in Figure 4.1, with third story being the roof. The typical floor-to-floor heights measured from center-of-beam-to-center-of -beam is 13 ft. The column bases are assumed as fixed supports at the ground level.

The floors are given as the composite construction of concrete and steel, and are comprised of wide-flange beams with the yield stress of 36 ksi. The floors provide a diaphragm action and are assumed to be rigid in the horizontal plane. Also, it is assumed that the inertial effects of each floor are transferred to each perimeter moment-resisting frame equally, thus each MRF resists one half of the seismic mass of the entire structure [56].

The seismic mass of the MRF is due to various components of the building, including the steel members, floor slabs, flooring and ceiling, mechanical /electrical works, floor partitions, roofing, and a penthouse located on the roof [56]. The seismic mass of the first and second levels is 65.5 kips-sec^2/ft. and the third level is 71.0 kips-sec^2/ft. The seismic mass of the entire structure

is 202 kips-sec^2/ft. [70]. For this study, only 2-D planar MRF structure in the N-S direction is analyzed, as three-dimensional effects can be neglected for simplicity. The N-S direction is chosen for our analysis because being the shorter side, the response experienced by the N-S frame will be much greater than the frame in the E-W direction being the shorter side. The baseline or original design including steel W-Section sizes of the N-S structure is as shown in Figure 4.1.

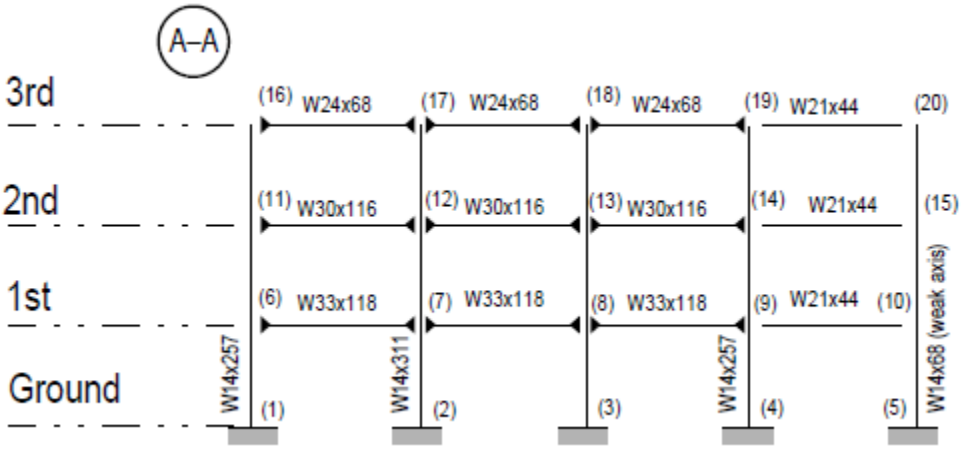

Figure 4.1: 3-Story Moment Resisting Frame (N-S elevation) [56]

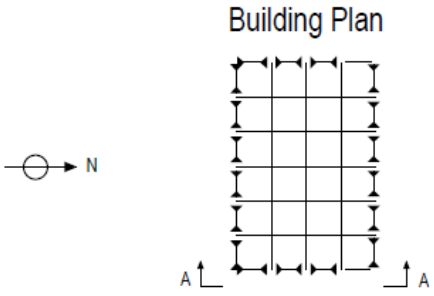

Figure 4.2: 3-Story Benchmark Building Plan [56]

4.2 OpenSees 2-D Linear Elastic Model

OpenSees Navigator (hereafter referred to as "OpenSees") is used in this study, as it offers a graphical user interface (GUI) pre- and post-processing framework for the OpenSees. The N-S MRF structure is modeled in OpenSees as a 2-D Frame by selecting the number of dimensions as two where each node of the structure contains three degrees of freedom, i.e. translation in X-direction, translation in Y-direction, and rotation about Z-direction. The English unit system (kips, inches, second) was adopted for the model and kept consistent with all the model input parameters.

The fixed boundary conditions at the ground level nodes were modeled by assigning fixed constraints in all three degrees-of-freedom using the Single-Point Constraint command in OpenSees. Further, the "EqualDOF" command was utilized to allow for the diaphragm action, by assigning equal translation in X-direction constraint at each floor level. Then, the seismic mass of each floor was lumped proportionally to the corresponding nodes. Note that since it was assumed each perimeter frame resists one-half of the entire seismic mass, the floor masses were divided by two and then distributed proportionally to each node; thus one-eighth of the floor mass were assigned at the interior nodes and one-sixteenth at the corner nodes.

The material chosen for the model was Steel01, which is a uniaxial bilinear steel material commonly used for performing linear elastic analysis. The yield stress was assigned as 50 ksi for columns and 36 ksi for beams, as per the baseline design. The frame members were assigned as "elasticBeamColumn" elements which are suitable for linear elastic analysis. However, for the furthest right beams (W21X44), "truss elements" were used instead to release the end moments and model the simple or pin connection behavior. Since, the furthest right columns of each floor (W14X68) are oriented in the weak-axis; the weak-axis section properties were chosen for these columns in the model. Additionally, second-order "P-delta" effects were simulated in the model

using leaning or “ghost” columns connected with rigid links at the right of the main frame as shown in Figure 4.3. The P-delta columns were modeled as “truss element” and assigned with gravity loads from the story weights. The final OpenSees model of the MRF is shown in Figure 4.3. The members are split into 7 groups as shown in Figure 4.3, therefore the optimization would consist of seven design variables.

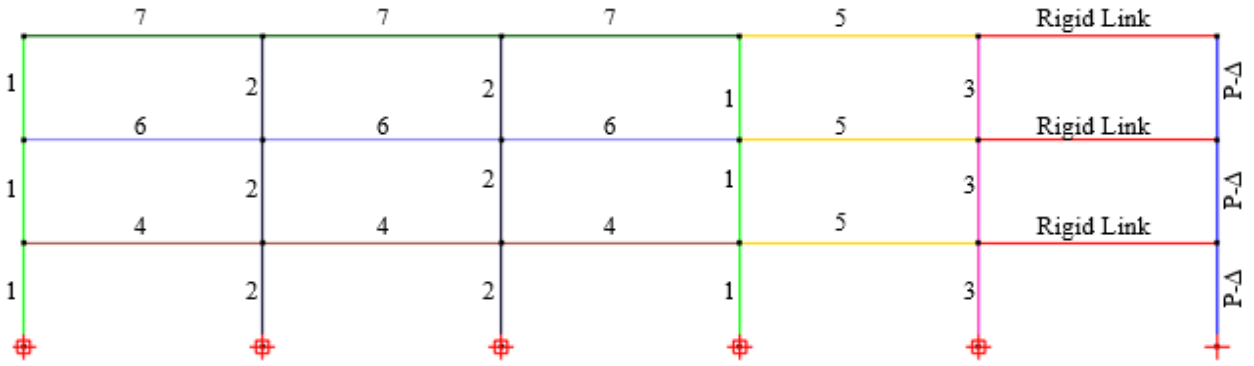

Figure 4.3: OpenSees Model for the 3-Story MRF

4.2.1 Model Validation

The OpenSees model was validated by performing the modal (Eigen) analysis and comparing the first three natural frequencies and periods of the 3-story benchmark structure [56]. The comparison is show in Table 4.1 and the first three modal shapes obtained in OpenSees is shown in Figure 4.4. The Eigen analysis results for the OpenSees model are similar to those previously obtained by Y. Ohtori, R.E. Christenson and B.F. Spencer, Jr., and S.J. Dyke [70], therefore, the OpenSees model for the 3-story MRF structure is accurate and good for further analysis.

Mode	Y. Ohtori, R.E. Christenson and B.F. Spencer, Jr., and S.J. Dyke [70]	OpenSees Eigen Analysis
	Natural Frequency (Hz)	Natural Frequency (Hz)
1st	0.99	0.990
2nd	3.06	3.057
3rd	5.83	5.831

Table 4.1: Modal (Eigen) analysis Comparison for 3-story MRF

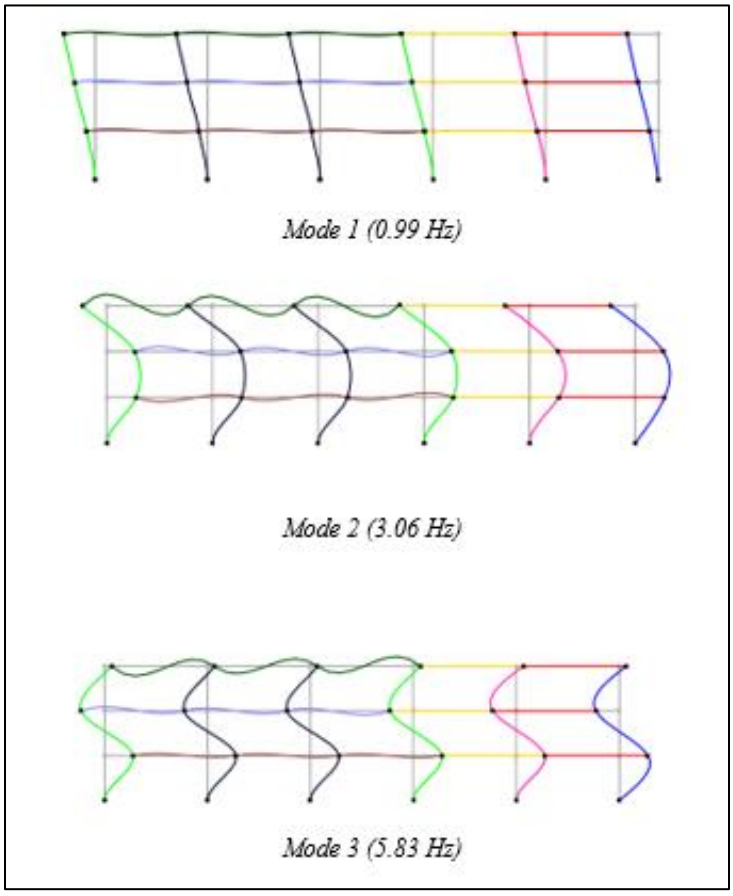

Figure 4.4: First three modal shapes for the 3-Story MRF

4.3 MATLAB-OpenSees Interface

The seismic design of the 3-story MRF frame requires modeling considerations and analysis procedures which are more advanced than the standard finite element modeling used for the benchmark problems in Chapter 3. These additional considerations include second-order (P-delta) effects, incorporating geometric and material nonlinearities, formulation of plastic hinges in the members, and predicting nonlinear and dynamic analysis response of structures. It would be both impractical and significantly inefficient to manually code the necessary analysis procedures. Therefore, an interface was created between MATLAB and OpenSees to prompt and automate the OpenSees analysis, and use its results for running the optimization in MATLAB.

OpenSees is primarily written in the object-oriented programming language C++ and uses Tcl as an interpreter for performing finite element analysis. OpenSees Navigator is a MATLAB based graphic user interface (GUI) that does pre- and post-processing for OpenSees, and it is available in a content-obscured form called P-code which allows to run OpenSees Navigator inside MATLAB [57]. OpenSees adds commands to Tcl for modeling- to create nodes, elements, loads, and constraints, analysis- to specify the analysis procedure, and output specification- to specify what needs to be monitored during the analysis [57]. Since Tcl uses a string-based command language; Tcl commands are incompatible with MATLAB syntax. Therefore, to prompt OpenSees for analysis during the optimization procedure, the MATLAB syntax must be converted to strings, so they be used as Tcl scripts by OpenSees.

The optimization algorithm randomly generates new variables (particles) resulting in new member properties at every iteration. Therefore, section sizes of the members are the main variables that would affect the OpenSees model for performing the finite element analysis, and rest of the model inputs and arguments remain unchanged throughout the iterative procedure. So, the approach is to define a structure and its section properties in MATLAB and convert it into Tcl script; prompt OpenSees for performing the finite element analysis, and then extract OpenSees results output back into MATLAB. In this way, OpenSees can be automatically prompted for analysis whenever the optimization algorithm generates a new particle during the iteration, the procedure of which is described in the following steps:

1) The original structure is modeled in OpenSees Navigator and its Tcl files are generated.
2) Create a folder and copy .M files, Tcl files, and OpenSees.exe into the same folder.
3) Generate a string matrix that contains the new section properties of the elements. However, the original Tcl command or rules shall remain unchanged; therefore, all the remaining commands and syntax rules should be included in the string matrix. Then, the existing Tcl element and/or Tcl section files shall be replaced/overwritten with this matrix using the "dlmwrite" function in MATLAB. Note that Tcl interprets the list of arguments or a subsequent character separated by whitespace, and so the number of blank spaces in between the list of characters does not impact the execution of the commands.
4) Prompt OpenSees for performing the analysis using the command: $!OpenSees.exe\ "filename".tcl$ [57]. Note, that the filename in the second part of the command should be the exact name of the Tcl file.
5) Once the OpenSees output is generated, the "dlmread" function is used to import the results into the MATLAB workspace.

Chapter 5: Seismic Design Optimization of 3-Story MRF

5.1 Introduction

In this chapter, the optimization will be performed for the 3-story moment resisting frame (MRF) for the Design Earthquake (475-year return period) loads, or seismic hazard level with 10% in 50 years probability of exceedance. Three separate analysis procedures will be considered for the optimization: the ASCE 7-10 equivalent lateral force procedure, ASCE 7-10 linear response history analysis, and FEMA 356 nonlinear static pushover analysis.

In the proceeding sections, OpenSees modeling considerations, assumptions, analysis steps, and optimization methods will be presented for each of the three analysis cases. Additionally, the problem-specific requirements for the interface between MATLAB and OpenSees will be discussed for the three analysis types. Then, the considered analysis procedure will be performed for the baseline or original design of the 3-story MRF structure, followed by the optimization to obtain an optimal design of the frame.

5.2 Linear Static Procedure

5.2.1 Equivalent Lateral Force Procedure (EFP):

The ASCE 7-10's-EFP- was followed to perform the seismic analysis and design optimization of the 3-story moment resisting frame structure. Since EFP is a linear static analysis, an OpenSees linear elastic model of the 3-story MRF, as shown in Chapter 4 (Figure 4.3), will be used for performing the analysis. The base shear and the seismic design parameters required for the analysis procedure for the 3-story MRF are obtained as follows:

Risk Category and Importance Factor, I_e:

ASCE 7-10 categorizes buildings and other structures into four levels (I-IV) for determination of wind, snow, earthquake loads based on risk to human life, economic loss, mass disruption of day-to-day civilian life or a potential threat or hazard to the community, in the event of failure of the structure. Since the occupancy of the 3-story benchmark building is for office use, a risk category of II is chosen for the seismic design [58]. Based on this risk category, a seismic importance factor, I_e is chosen to be as 1.0 [59].

Period Determination, T:

The fundamental period, T of the 3-story MRF was determined to be 1.01s from the Eigen analysis in Chapter 4. An upper limit for the period ($C_u T_a$) was determined using Eq. 2.9 which came out to be 0.73s; therefore $C_u T_a$ is used for computing the seismic response coefficient, C_s and seismic base shear, V [27]. Note that these period values are as per the structural properties of the baseline or original design.

Seismic Design Response Spectrum:

The ASCE 7-10 mapped spectral acceleration parameters, S_s and S_1can be electronically obtained from the United States Geological Survey (UGGS) Seismic Design Maps tool [60]. The tool requires the inputs including the design code reference, the building location or site coordinates, and the classification of the soil site. The spectral acceleration parameters and the design response spectrum for the 3-story MRF structure obtained from the USGS website are shown in Figure 5.1 and Figure 5.2. The design spectral acceleration parameters S_{DS} and S_S are obtained as 1.622g and 0.853g, respectively.

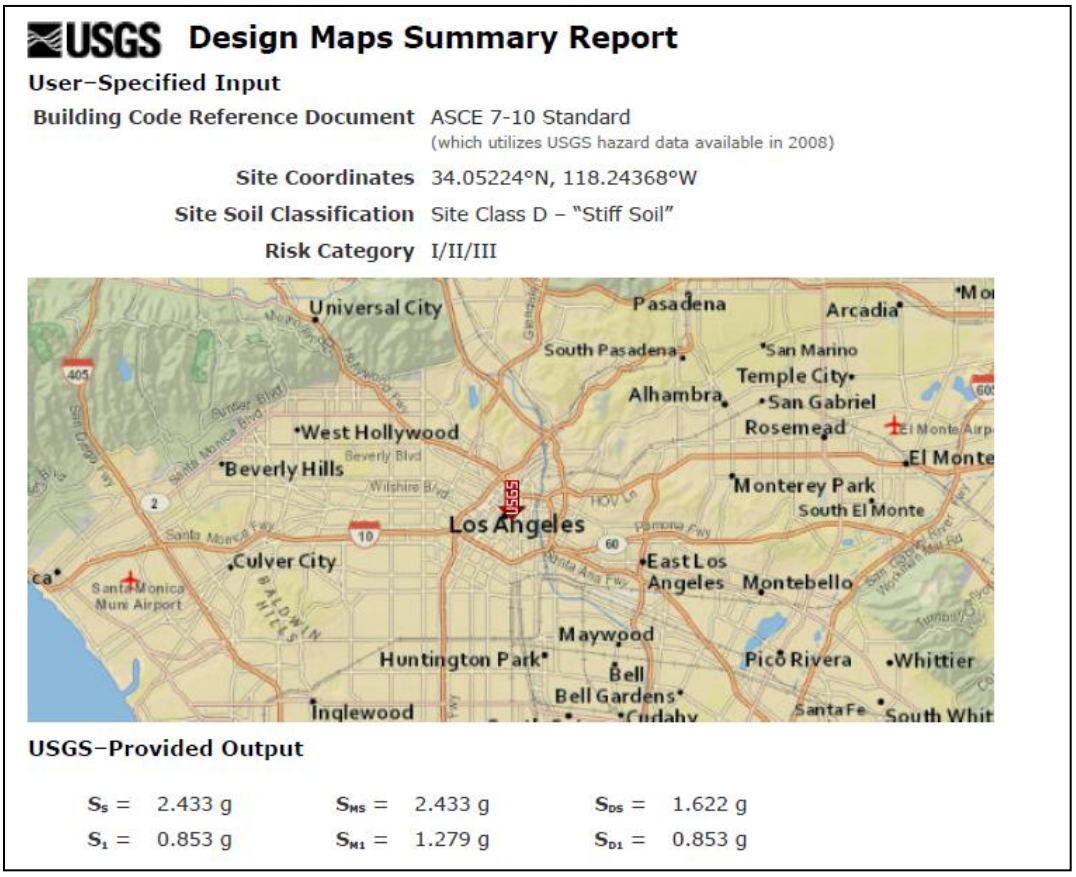

Figure 5.1: ASCE 7-10 Spectral Acceleration Parameters for the 3-story Benchmark Building [60]

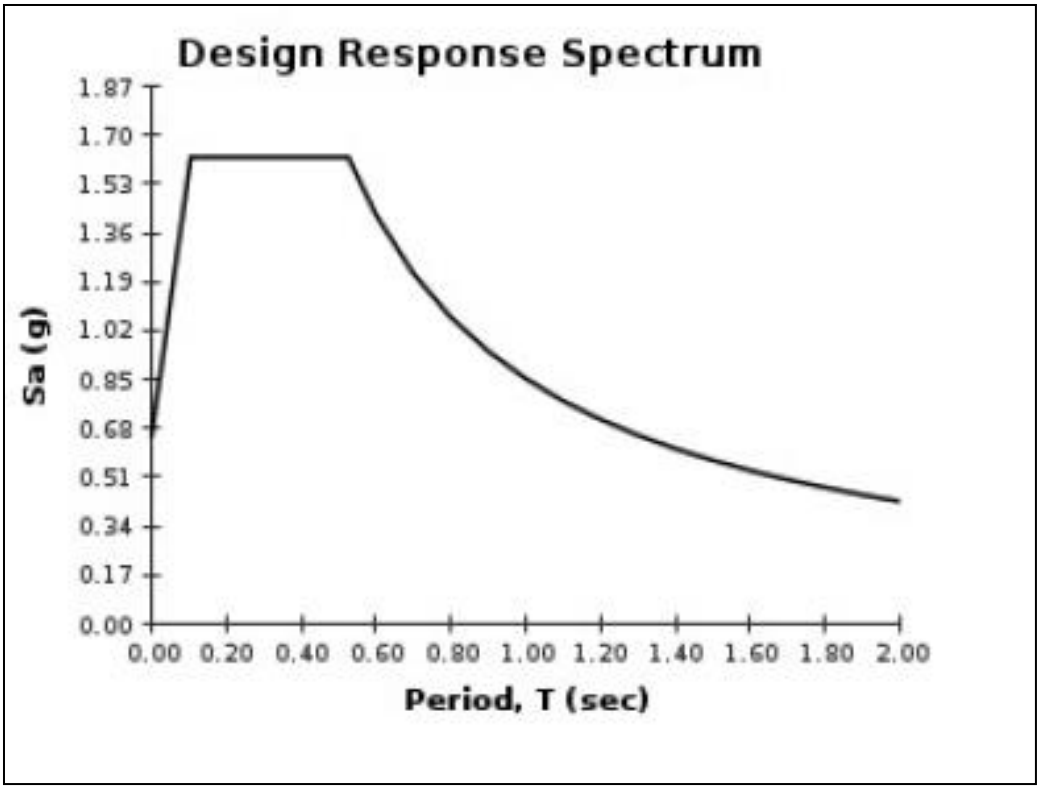

Figure 5.2: ASCE 7-10 Design Response Spectrum for the 3-story Benchmark Building [60]

Seismic Design Coefficient and Factors:

The empirical factors required as per the seismic design criteria are obtained from ASCE 7-10 [61] (Appendix A). For the 3-story moment resisting frame, the response modification factor, R, displacement amplification factor C_d, and overstrength factor, Ω_o, were obtained to be as 8, 5.5, and 2.5, respectively.

Seismic Base Shear, V:

The effective seismic mass of the 3-story benchmark building is given as 202 kips-sec^2/ft, which converts to a seismic weight, W of 6500 kips. Since each MRF resists one half of the seismic weight of the entire structure, the seismic weight is reduced by half (W=3250 kips), for the base shear calculation. Having obtained the values of T, S_{DS}, S_{D1}, R, and I_e, the seismic response coefficient, C_s is determined to be as 0.1451 as per Eq. 2.14 and in accordance with the minimum

and maximum limits specified in the code [30]. Thus, using Eq. 2.13, the seismic base shear, V comes out to be 471.5 kips.

The seismic and gravity analysis was performed for the baseline design of the 3-story MRF structure using OpenSees. The seismic story forces were determined using the vertical distribution of seismic base shear (Eq. 2.15 and Eq. 2.16), as summarized in Table 5.1. Note that different load combinations are used for beams and columns to meet the capacity design principles. For columns, the load combination with amplified seismic forces is considered (Eq. 2.18). For beams and story drift determination, basic load combination is considered. (Eq. 2.17a) The effective length factor, K for determining the available strengths in columns, is taken as unity as recommended in the AISC Seismic Provisions [62].

Level	**w_x (kips)**	**h_x(ft.)**	**$w_x h_x^k$**	**C_{vx}**	**F_x (kips)**	**$\Omega_O E$ (kips)**
Roof	1142	39	44538	0.5386	254.0	635
Level 2	1053.6	26	27393.6	0.3158	148.9	372.25
Level 1	1053.6	13	13696.8	0.1456	68.7	171.75

Table 5.1: Vertical Distribution of Base Shear and Story Seismic Forces

The seismic design load combinations defined in Eq. 2.17 and Eq. 2.18 were used to obtain the factored gravity load values, and are provided in Table 5.2. The floor dead loads and live loads were obtained from the ASCE 7-10 codes. Note that a factor of 0.5 is used for live loads, as the minimum uniformly distributed live loads for an office building in less than 100psf [29]. Additionally, the roof live loads are assumed to be the same as the floor live loads because of the penthouse located on the roof.

Level	Factored Dead Load, D (k/ft.)	Factored Live Load, L (kip/ft.)	Factored Cladding Loads (kips)	
			Intermediate	Corner
Roof	0.82	0.3	46.49	30.34
Floors	1.05	0.3	51.83	34.91

Table 5.2: Gravity Loads used in the Linear Static analysis

The linear static analysis was performed in OpenSees and the peak roof displacement was determined to be 9.34 in. which corresponds to a 1.92% drift ratio. The inter-story drift for the first story, second story, and roof were obtained as 2.53 in., 3.57 in., and 3.23 in., respectively. The inter-story drift for the first, second, and roof correspond to the inter-story drift ratios of 1.62%, 2.29%, and 2.07%, respectively. The combined column strength ratios and beam rotations obtained from the analysis are shown in Tables 5.3. As shown in the table, the highest combined strength ratio for columns was attained to be as 1.34 in member 2 which is the inner column of the bottom story.

From the analysis, it is observed that the inter-story drift ratio limits (2.0% as per Table 2.3) and the AISC LRFD column interaction ratios (Eq. 2.3 and Eq. 2.4) are violated for the baseline design. However, there is no knowledge about the assumptions, seismic design criteria or specifications undertaken by the engineers for the original design; therefore, the results have to be taken as it is. Also, since the analysis results are sensitive to selection of design parameters, as discussed in Chapter 7 of this study, whether the baseline design is adequate or not is a moot question.

Member	**Column Strength Check Ratio (<1.0)**	**Member**	**Beam Plastic Rotations (rad.) (<0.04)**
1	1.19	16	0.029
2	1.35	17	0.023
3	1.34	18	0.027
4	1.27	19	0.041
5	0.36	20	0.029
6	0.66	21	0.025
7	1.02	22	0.028
8	1.02	23	0.037
9	0.75	24	0.03
10	0.08	25	0.026
11	0.37	26	0.027
12	0.65	27	0.034
13	0.64	-	-
14	0.45	-	-
15	0.04	-	-

Table 5.3: EFP Column Strength Design Checks and Beam Rotations

5.2.2 Optimization

For the linear static case, the HPSO algorithm was used for optimization. To implement the optimization algorithm to the equivalent lateral force procedure for the seismic design optimization of the benchmark structure, a code was developed in MATLAB that is capable of automating the analysis procedure using OpenSees while conforming to all the analysis considerations and ASCE 7-10 seismic design criteria discussed above. The three main analysis considerations required in the optimization procedure included period determination, calculation of base shear, load combinations, and drift determination.

Period Determination:

It is known that natural frequencies and period of the structure depend on the stiffness properties of the members; therefore, the period values shall be determined at every iteration for every new particle generated per iteration. Thus, Eigen analysis is performed at every iteration using the MATLAB-OpenSees interface technique developed in Chapter 4.

Base Shear Calculation:

Since the seismic response coefficient, C_s relies on period determination; the base shear value has to be updated at every iteration (as per Eq. 2.13), due to the change in the period value. As a result; the OpenSees load file has to be overwritten with the updated lateral seismic forces values at every iteration. Thus, the applied seismic loads do not remain constant and are updated every time a new particle are generated during the optimization.

Load Combinations:

Two different loads combinations are considered in the above procedure, so two analyses were performed at every iteration, i.e., one with amplified seismic loads ($\Omega_o E$) to determine required forces in columns and second with basic load combination ($1.0\ E$) to determine beam rotations and story drifts.

Drift Determination:

For determining compliance with story drift limits, it is allowed to determine the elastic drifts, δ_{xe}, using seismic design forces based on the computed fundamental period of the structure without the upper limit ($C_u T_a$) [40]. Therefore, for cases where the computed fundamental period exceeds the upper limit ($C_u T_a$), the seismic base shear is calculated based on the computed fundamental period. However, if the computed fundamental period comes out to be less than or equal to the upper limit (($C_u T_a$), the base shear will be the same.

Variable Constraints:

For the optimization of the frame, different variable boundaries were considered for the columns members to make the optimization more efficient and make the optimal design more feasible. Since minor axis buckling usually govern for all doubly-symmetric cross-sections; the most efficient column section for axial loads are those with almost equal radius of gyration values about both x-axis and y-axis ($r_x = r_y$), therefore W8, W10, W12, and W14 are typically used for columns. However, for the seismic design of steel buildings, W14s are the most efficient column sections because under seismic loads, columns experience high lateral drifts and develops significant moments, and W14s ae the heaviest sections available that has seismically compact flanges. Therefore, 36 AISC W14 section sizes were considered as discrete design variables in the optimization.

Optimization Parameters and Constraints:

The PSO parameters and the design constraints considered for the seismic design optimization of the 3-story MRF structure are shown in Table 5.4. The PSO parameters were selected using the guess-and-check approach and were found to be the most efficient for the algorithm. The design constraints considered in the optimization include: peak roof drift limit, inter-story drift limit, combined strength ratio for columns, and beam plastic rotations specified in the AISC Seismic Provisions [63].

Problem Constraints		**PSO Parameters**	
Variables	273 AISC W-shapes (Beams) 36 AISC W14s (Columns)	No. of particles	25
Max. Roof Drift (Ratio)	9.36 in. (2.0%)	Max. Iterations	1000
Max. Inter-Story Drift (Ratio)	3.14 in. (2.0%)	w	0.8
Beam Plastic Rotations	0.04 rad.	c_1, c_2	2, 2

Table 5.4: EFP Optimization Parameters and Problem Constraints

Optimization Results:

Figure 5.3 shows the convergence graph for the seismic design optimization of the of the benchmark building for the equivalent lateral force procedure (linear static) case. The optimal weight of the design was obtained to be as 91344 lb. For the optimal frame, the inter-story drifts are shown in Table 5.5 and, combined strength ratios and beam rotations are shown in Table 5.6. It can be observed that in the optimal frame, the top inter-story drift of 3.1178 in. is very close to the allowable inter-story drift of 3.12 in. Also, most of the bottom story columns have their combined strength ratios close to 1. This indicates that both story drifts and strength constraints equally dominate the optimal design of the structure for the linear static analysis case. The comparison of the baseline design and the optimal member sizes is shown in Table 5.7. It is

apparent that the weight of the optimal design will be more than that of the baseline design, as the results for the baseline design did not comply with the ASCE 7-10 seismic design criteria.

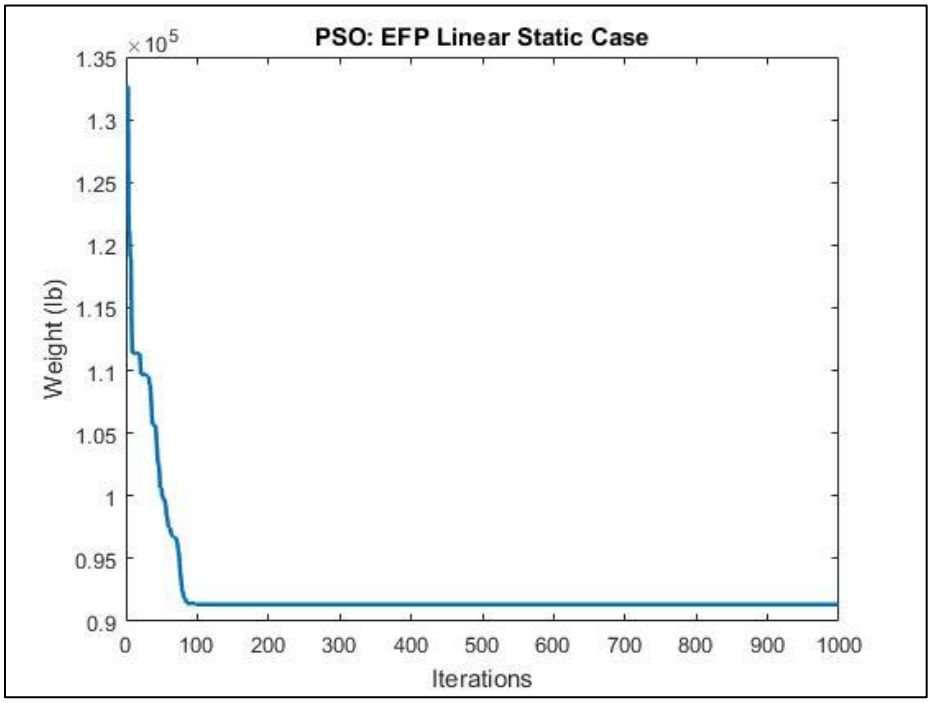

Figure 5.3: HPSO graph for Seismic Design of 3-Story Benchmark Building (Linear Static Case)

Story	**Inter-story Drifts (in.)**
	Allowed = 3.12 in.
First	2.0772
Second	2.6362
Roof	**3.1178**

Table 5.5: Inter-Story Drifts for Optimal Design (Linear Static Case)

Column No.	Column Strength Check Ratio (<1.0)	Beam No.	Beam Plastic Rotations (rad.) (<0.04)
1	0.9045	16	0.013
2	**0.9942**	17	0.013
3	0.9927	18	0.013
4	0.9837	19	0.027
5	0.902	20	0.019
6	0.6241	21	0.019
7	0.7232	22	0.019
8	0.7189	23	0.023
9	0.6982	24	0.012
10	0.5649	25	0.011
11	0.5437	26	0.011
12	0.639	27	0.020
13	0.6359	-	-
14	0.6054	-	-
15	0.2558	-	-

Table 5.6 Column Strength Ratios and Beam Plastic Rotations for Optimal Design (Linear Static Case)

ASCE 7-10 Equivalent Lateral Force Procedure			
Group	**Member**	**Baseline Design**	**Optimal Design**
1	Column	W14X257	W14X257
2	Column	W14X311	W14X426
3	Column (Weak Axis)	W14X68	W14X30
4	Beam	W33X118	W40X149
5	Truss	W21X44	W18X35
6	Beam	W30X116	W36X182
7	Beam	W24X68	W21X44
	Weight (lb)	78096	91344

Table 5.7 Optimal Design for 3-Story Benchmark Building (Linear Static Case)

5.3 Linear Dynamic Procedure

5.3.1 Ground Motions Record

The ground motion time history records were obtained from the Pacific Earthquake Engineering Research Center (PEER) website. A suite of seven LA ground motions records, as shown in Table 5.8 were considered for the linear response time-history or linear dynamic (LD) analysis of the 3-story MRF structure in OpenSees.

EQ Code	Description	Magnitude	Distance (km)	No. of Points	Time Step (s)	PGA (cm/sec^2)	PGA (g)
25	fn 1994 Northridge	6.7	7.5	2990	0.005	851.62	0.87
26	fp 1994 Northridge	6.7	7.5	2990	0.005	925.29	0.94
33	fn Elysian Park (simulated)	7.1	10.7	3000	0.010	767.26	0.78
35	fn Elysian Park (simulated)	7.1	11.2	3000	0.010	973.16	0.99
36	fp Elysian Park (simulated)	7.1	11.2	3000	0.010	1079.30	1.10
37	fn Palos Verdes (simulated)	7.1	1.5	3000	0.020	697.84	0.71
39	fn Palos Verdes (simulated)	7.1	1.5	3000	0.020	490.58	0.50

Table 5.8 Ground Motion Records for LD Analysis

These ground motions are scaled such that the average value of the 5 percent damped response spectra for the seven ground is not less than the design response spectrum (Figure 5.2) for the site between the periods 0.2 T and 1.5 T [43]. A MATLAB code was generated to compute the acceleration response spectrum for an SDOF system using Newmark's method [64]. Then, by using guess-and-check approach, the scaling factors were obtained for the seven ground motion values such that the mean response spectrum of the seven response spectra for the scaled ground motions were above the design response spectrum within the required period range, as shown in the results in Figure 5.4. Note, the fundamental period values will change for every new particle generated, however, since it would be infeasible to automate this guess and check procedure, an

assumption is made that the mean response for every particle would always meet the criteria, or would never be in a period range in which the mean response is lower than the design response spectrum.

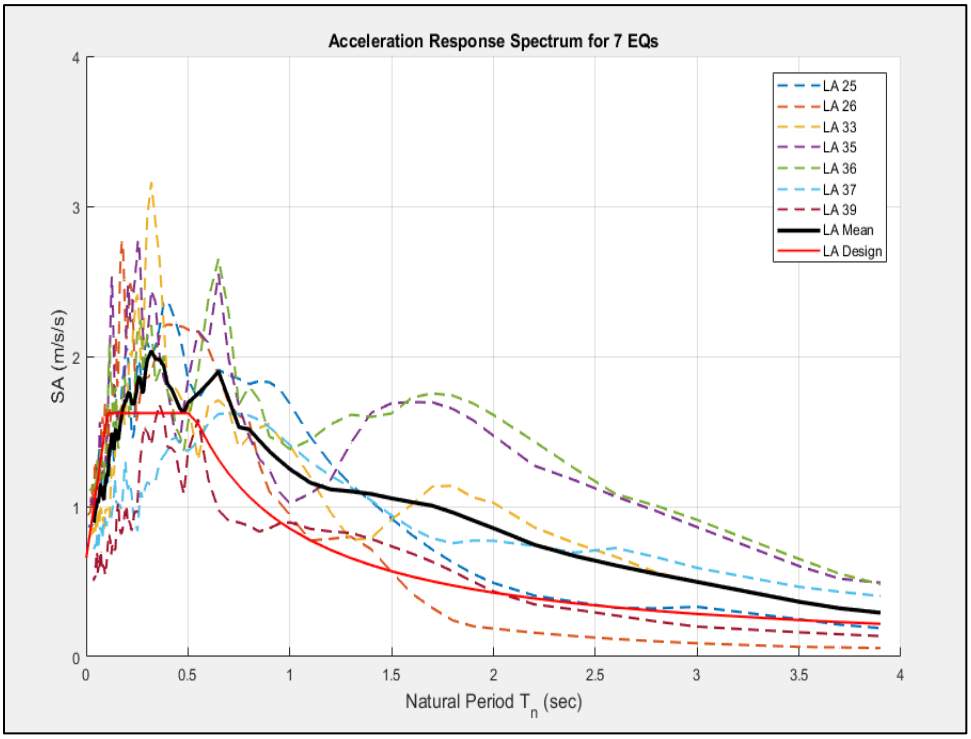

Figure 5.4: MATLAB Plot of Scaled EQs , Mean, and Design Acceleration Response Spectrum

5.3.2 ASCE 7-10 Linear Response Time-History Analysis

The linear elastic model used in the preceding sections is used for the incremental dynamic or transient analysis case in OpenSees for the 3-story MRF structure. First, the load pattern for the time history analysis were defined by importing the scaled ground motion values path files in OpenSees. The number of data points and time steps for each time series are as provided Table 5.8. Since the acceleration time history of the recorded ground motions are in units of g, the load values were factored with 386 in^2/sec.

The integrator type for the numerical evaluation of the dynamic response was performed using the Newmark method of integration. In IDA procedures, finer time step increments are recommended for robustness and to resolve convergence issues of the numerical integration [65]. Thus, the analysis increment time step was selected to be 0.001 for each transient analysis.

The damping was assigned to the OpenSees model using the mass and stiffness proportional Rayleigh damping parameters. The damping ratio for the first two modal frequencies were set to 5%. The Rayleigh mass proportional parameters $alphaM$ and stiffness proportional parameter $betaK$ were determined to be 0.4699 and 0.0039, respectively for the baseline 3-story MRF structure.

The analysis was performed for the baseline benchmark structure for the seven analysis cases. The force responses and story drifts are multiplied by the factors I_e/R and C_d/R, respectively, for each analysis case. Then, the design forces and drifts are determined by taking an average of the scaled force and displacement responses obtained from the analyses. The peak roof displacement was found to be 12.33 in., which is approximately 32% larger than peak roof displacement obtained in the EFP or linear static case. Table 5.8 shows the comparison of the inter-story drifts obtained from the transient analysis and from the linear static case (see section 5.2.1). The allowable inter-story drift limit for the frame is determined to be 3.9 in. Table 5.9, and Tables 5.10 and 5.11 shows the comparison of the obtained combine column strength ratios and beam plastic rotations for the two analysis cases, respectively.

Story	Inter-story Drifts (in.)	
	EFP or Linear Static Analysis	Linear Dynamic Analysis
	Allowed = 3.12 in.	Allowed = 3.9 in.
1	2.5322	3.518
2	3.5743	4.7252
Roof	3.2335	4.0878

Table 5.9: Inter-story Drift Comparison for Linea Static and Linear Dynamic Analysis Case

Column Strength Check Ratio (<1.0)		
Column No.	EFP or Linear Static Analysis	Linear Dynamic Analysis
1	1.18	1.25
2	1.34	1.35
3	1.33	1.35
4	1.26	1.25
5	0.35	0.17
6	0.65	0.73
7	1.01	1
8	1.01	1
9	0.74	0.72
10	0.08	0.04
11	0.37	0.46
12	0.64	0.68
13	0.64	0.68
14	0.45	0.46
15	0.04	0.03

Table 5.10: Column Strength Ratio Comparison for Linear Static and Linear Dynamic Analysis Cases

Beam Plastic Rotations (rad.) (<0.04)		
Beam No.	**EFP or Linear Static Analysis**	**Linear Dynamic Analysis**
16	0.029	0.022
17	0.023	0.018
18	0.027	0.022
19	0.041	0.033
20	0.029	0.022
21	0.025	0.019
22	0.028	0.022
23	0.037	0.029
24	0.03	0.023
25	0.026	0.021
26	0.027	0.023
27	0.034	0.027

Table 5.11: Beam Plastic Rotations Comparison for Linear Static and Linear Dynamic Analysis Cases

5.3.4 Optimization

For linear dynamic case, the standard PSO algorithm was found to be more efficient than the HPSO technique, as HPSO initializes the swarm within the feasible region and therefore its computation time is significantly higher. A MATLAB code was developed to meet the above analysis considerations and the seismic design criteria for the linear response time-history procedures as specified in Section 2.3.4. It shall be noted that in the transient analysis case, the seismic forces remain constant throughout the optimization iterations unlike in the previous case of equivalent lateral force procedure. However, since the damping depends on the natural frequencies of the structure; Rayleigh damping parameters had to be determined at every iteration. Therefore, for every new particle, the OpenSees Tcl file containing damping parameters had to be overwritten following the interface procedure in Chapter 4.3.

The variable and problem constraints considered in this analysis were same as the ones considered in the linear static case (see Table 5.3), with an exception for the inter-story drift (ratio), as the allowable drift limit in the dynamic procedures is 2.5% or 3.9 in. [35]. Figure 5.5 shows the convergence graph for the linear dynamic analysis case. The optimal weight of the design was obtained to be as 100182 lb which is approximately 10% higher than the optimal weight of the linear static case. For the optimal design, the inter-story drifts are shown in Table 5.12 and, combined strength ratios and beam rotations are shown in Tables 5.13 and 5.14, respectively. The optimized frame has the top inter-story drift of 3.864 in. which is very close to its upper bound of 3.9 in. Also, the bottom story interior columns (Column No.2 and 3) have their combined strength ratios close to 1. This indicates that both story drifts and strength constraints equally dominate the optimal design of the structure for the linear dynamic analysis case.

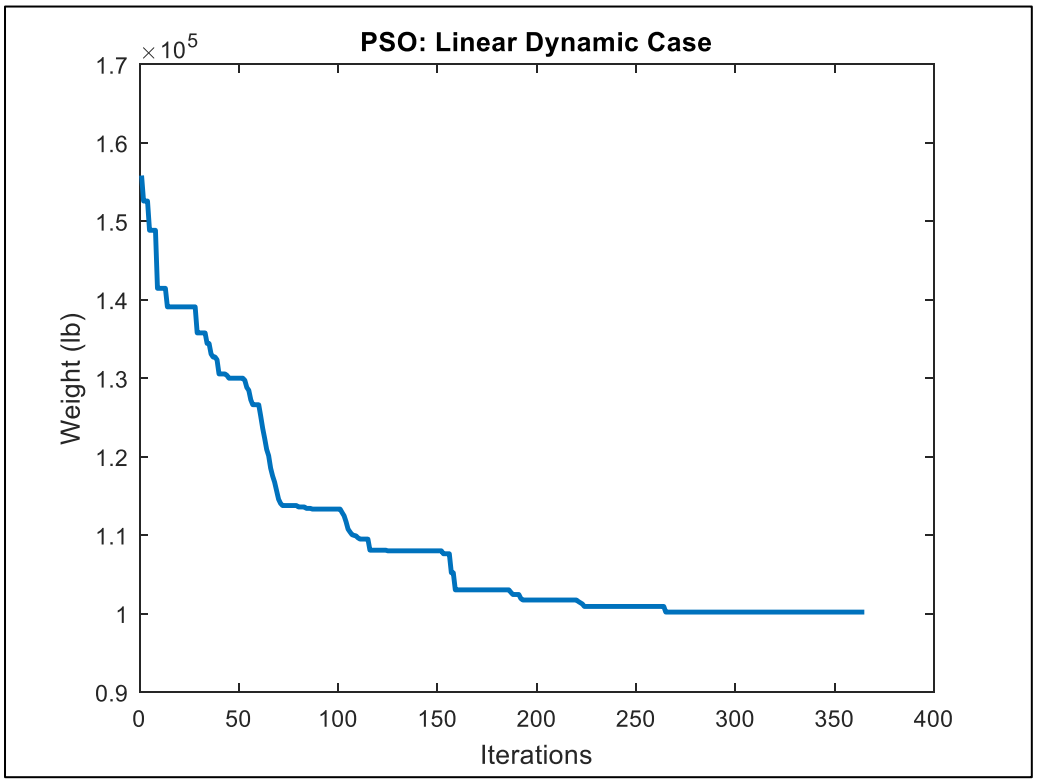

Figure 5.5: PSO Convergence Graph for Seismic Design of 3-Story Benchmark Building (Linear Dynamic Case)

Story	Inter-story Drifts (in.)	
	EFP or Linear Static Analysis	**Linear Dynamic Analysis**
	Allowed = 3.12 in.	Allowed = 3.9 in.
1	2.0772	2.3555
2	2.6362	2.8532
Roof	**3.1178**	**3.8674**

Table 5.12: Inter-story Drift Comparison for Optimal Designs

Column Strength Check Ratio (<1.0)		
Column No.	**EFP or Linear Static Analysis**	**Linear Dynamic Analysis**
1	0.9045	0.9647
2	**0.9942**	0.9982
3	0.9927	**0.9983**
4	0.9837	0.9625
5	0.902	0.7685
6	0.6241	0.6573
7	0.7232	0.7228
8	0.7189	0.7223
9	0.6982	0.6613
10	0.5649	0.4861
11	0.5437	0.6972
12	0.639	0.7851
13	0.6359	0.7847
14	0.6054	0.7050
15	0.2558	0.2219

Table 5.13: Column Strength Ratio Comparison for Optimal Designs

Beam Plastic Rotations (rad.) (<0.04)		
Beam No.	**EFP or Linear Static Analysis**	**Linear Dynamic Analysis**
16	0.013	0.0115
17	0.013	0.0110
18	0.013	0.0115
19	0.027	0.0202
20	0.019	0.0111
21	0.019	0.0106
22	0.019	0.0111
23	0.023	0.0214
24	0.012	0.0294
25	0.011	0.0292
26	0.011	0.0293
27	0.020	0.0292

Table 5.14: Beam Rotations Comparison for Optimal Designs

5.4 FEMA-356 Nonlinear Static Procedure

5.4.1 OpenSees Nonlinear Model

The nonlinear static procedure requires a nonlinear model that directly incorporates the nonlinear load-deformation characteristics of individual components and elements; and explicitly includes their nonlinear behavior using full backbone curves including strength degradation and residual strengths. This is achieved with the help of advanced nonlinear modeling and analysis capabilities using a wide range of material models and nonlinear elements. Thus, a separate 2-D nonlinear model of the 3-story moment resisting frame was built in OpenSees for the nonlinear static analysis case. The modeling considerations undertaken while building a nonlinear OpenSees model are discussed below.

Nonlinear Material

For the nonlinear model of the benchmark building, *Steel02* is chosen which follows the stress-strain relationship of the well-known "Guiffre-Menegotto-Pinto Model" with Isotropic Strain Hardening" [57]. The parameters used for this material model as shown in Figure 5.6 are selected as per the recommended values by one of the OpenSees developers, Dr. Fillip Filippou [66]. The strain hardening ratio, b is taken as 3% as specified in the FEMA-356 guidelines [67]. The transition parameters R0, cR1, cR2 are related to the smoothness of the transition from elastic to plastic regions [66].

Define Steel02 Material		
Material Name :	Beam	Add
Yield Stress (Fy) :	36	
Modulus of Elasticity (E) :	29000	
Hardening Ratio (b) :	0.03	
Transition Parameter (R0) :	19	
Transition Parameter (cR1) :	0.925	
Transition Parameter (cR2) :	0.15	

Figure 5.6: OpenSees *Steel02* Material Input Parameters

Nonlinear Elements:

There are two types of nonlinear modeling approaches- one is simulating concentrated plasticity in the members by using rotational springs at the end, and second is distributed plasticity concept where the plastic behavior can be developed over the finite length of the elements. The main advantages of the concentrated plasticity approach are that they are simple and very computationally efficient; however, it requires moment-rotation relationships to be explicitly defined in the model for all individual members and they don't capture P-M interaction which is usually critical for columns [68]. Whereas, for the distribution plasticity model the advantages include capturing of plasticity along the length of the member and the P-M interactions, but they use fiber sections, for which the number of fiber discretization can impact the results.

The concentrated plasticity model was not considered in this study, as this would require explicit modeling of the moment-rotation relationships of individual beam-column connections, and these modeling parameters are based on experimental results. Although there are available tools that contain the database of these modeling parameters, however, it would have been computationally inefficient and impractical to consider them in the optimization process, as this

would have required an interface between MATLAB and the database, so that the moment-curvature relationships can be automatically simulated in OpenSees. Therefore, distributed plasticity model will be used instead which is based on stress-strain relationships of fiber sections of individual elements. These elements can be modeled by selecting *nonlinearBeamColumn* elements in OpenSees.

Fiber Sections

According to Kostic and Filippou [68], discretization of wide-flange cross-sections with 12 fibers gives remarkable accuracies in the estimates of the local response, thus, each wide-flange I section used in the model is discretized into 12 fibers- 4 in each flange, and 4 along web depth.

5.4.2 FEMA 356 Nonlinear Static Analysis

Pushover Curve

The pushover analysis was performed using the nonlinear OpenSees model for the benchmark structure, as per the analysis requirements discussed in Section 2.3.6. The pushover curve was obtained for the baseline MRF frame and was compared with the pushover curve obtained for the linear elastic model, as shown in Figure 5.7. As expected, the elastic stiffness or initial slopes of the two pushover curves are close.

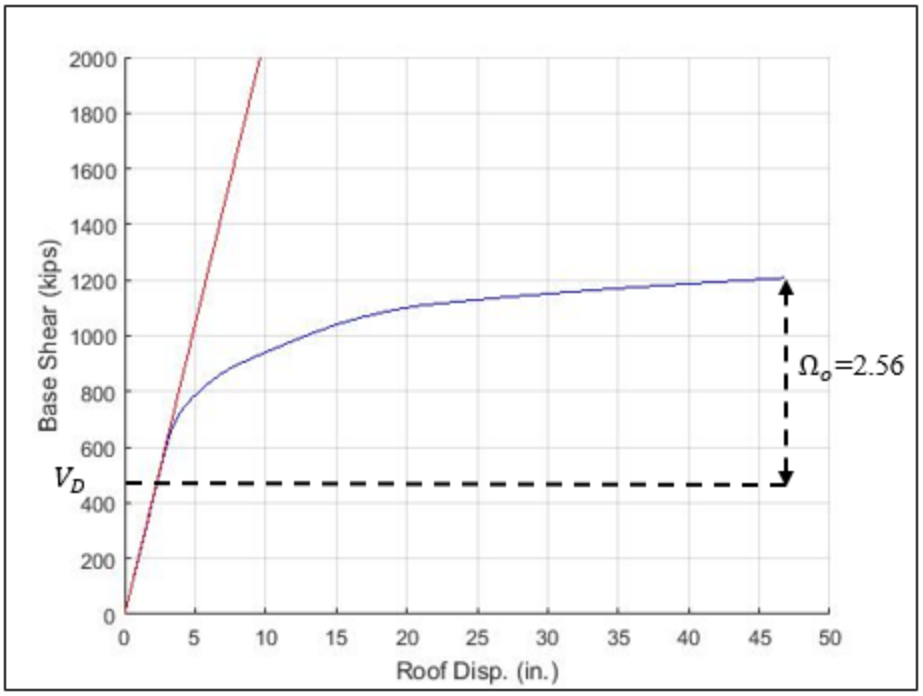

Figure 5.7: Pushover Curves for Linear Elastic and Nonlinear Model

As seen in the above figure, the overstrength factor Ω_o obtained from the design base shear level, V_D and the maximum base shear was determined to be 2.56, which is very close to the empirical overstrength factor of 2.5 specified in the ASCE 7-10 code. From these comparisons, it can be concluded that the OpenSees nonlinear model is reasonable and fit for the nonlinear static analysis.

Idealization of Pushover Curve

As discussed in Section 2.3.6, a bilinear idealization of the pushover curve is required to determine effective yield strength, V_y and effective lateral stiffness, K_e, for which the line segments on the idealized pushover curve must be placed using an iterative graphical procedure that approximately balances the areas below and above the curve. Therefore, the challenge was to formulate the iterative graphical procedure in MATLAB, so that the idealization procedure could

be automated, and the above parameters required for the nonlinear static analysis could be determined during the optimization.

The main concept behind formulating the idealization procedure in MATLAB was to treat slopes of the two line segments as variables and perform iterations until the difference of the areas above and below the curve ("Net Area") evaluated at each iteration, were minimal or close to zero. One considered approach involved coming up with a feasible range for each of the two slopes that can be discretized into N number of increments and then evaluate the Net Area for every possible combination of the two slopes. Then, the pair which yields the minimum Net Area would define the location of the two line segments that approximately balances the areas below and above the pushover curve. However, this approach was very computationally intensive, as this involved performing computations to obtain the bounded areas N^2 number of times, and yielded imprecise results.

As an alternative to the above approach, the PSO optimization technique was developed and applied to the above problem, where the Net Area was minimized by searching for the optimal values of the slopes for the two line segments. The Net Area was selected as the objective value function and the two slopes were assigned as the variables (particles). Since there are finite number of solutions possible, as the line segments must be within the curve region; the variables had to be kept within the feasible boundaries. Therefore, to bypass the nonexistent solutions during the optimization procedure and to come up with the feasible ranges for the variables, the following were assumptions and conditions were established:

- The fixed points for the two line segments include the point of origin (0, 0) and the base shear at target displacement level, δ_t, as per Figure 2.5.
- The slope of the first line segment is less than or equal to the initial lateral stiffness value K_i, i.e., slope of the elastic region of the pushover curve.
- The intersection points 1, 2, and 3, as shown in Figure 5.8, shall follow the order $1 > 2 > 3$, and shall be treated as optimization constraints.

Figure 5.8 shows the comparison of the idealized pushover curves obtained from the two approaches along with their computational times and the obtained net area results. It is evident that the optimization approach was found to be highly efficient and accurate with Net Area almost closer to zero, than the previous approach.

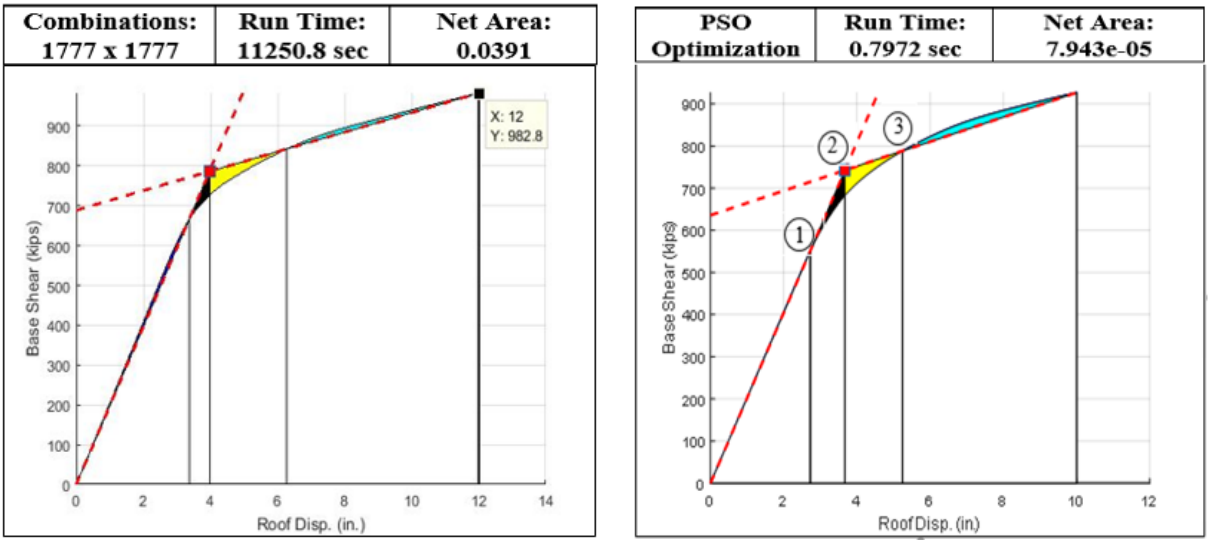

Figure 5.8: Idealization of Pushover Curve Comparison

Target Displacement

The idealization procedure of the pushover curve needs to know the target displacement point δ_t (Figure 2.5), however the target displacement is initially unknown for the idealization procedure to begin with. Therefore, an iterative procedure was used, where an initial point of target displacement is assumed, and idealization procedure is repeated until the target displacement, δ_t, remains unchanged. The iteration steps can be explained as follows:

1) Assume an initial value for target displacement, $\delta_{t,i}$. This can be taken as the maximum displacement of the pushover curve.
2) Perform the bilinear idealization procedure corresponding to the initial $\delta_{t,i}$
3) Determine the parameters V_y, K_e, and T_e, and the target displacement, δ_t as per Eq. 2.20
4) Use the above target displacement δ_t as the new initial guess for the target displacement $\delta_{t,i}$ and repeat Steps 1-3 until δ_t and $\delta_{t,i}$ are approximately equal.

The above iterative procedure could make the optimization very computationally intensive. It was found that in most of the cases, two initial guesses or three iterations were sufficient to obtain the final value for δ_t. Also, since it is almost impossible to have the two values, i.e., $\delta_{t,i}$ and δ_t to be exactly equal, more number of iterations would not have made any difference, and therefore three iterations were enough to meet a tolerance limit of somewhere between 0 and 1. Figure 5.9 shows the convergence of the difference between the initial and final values of target displacement for three iterations, and reinstates the assumptions claimed above.

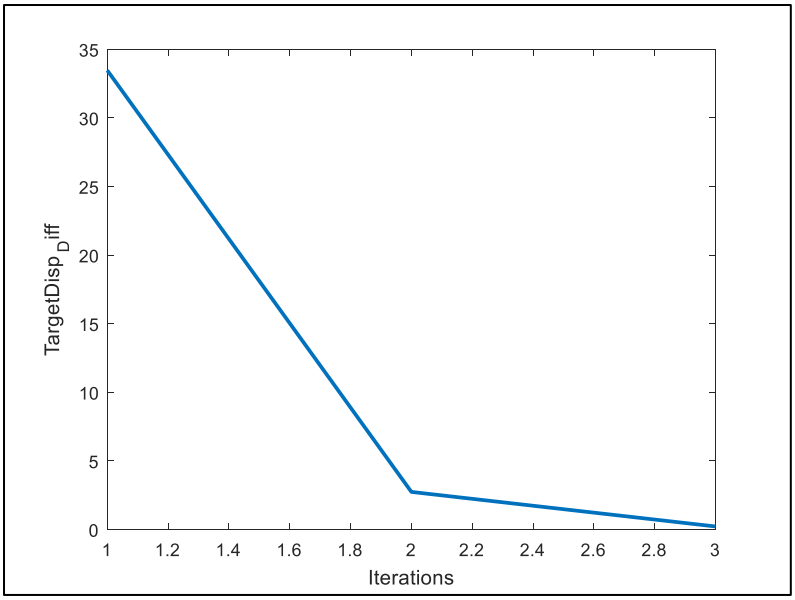

Figure 5.9: Convergence of Target Displacement Difference

Thus, following the above procedures for the baseline MRF structure, the effective yield strength, V_y, and effective lateral stiffness, K_e, were determined to be 445.2145 kips and 202.0139 kips/in, respectively. Eq. 2.20 gives the effective period, T_e as 1.0216 s. The response spectral acceleration, S_a was determined to be 0.8349 using FEMA 356's general response spectrum equations for the design level earthquake for the same acceleration parameters (S_s and S_1) used in the EFP linear static case (Section 5.2). Using the coefficient values of C_0, C_1, C_2 and C_3 as 1.2, 1,1, and 1, respectively, as per Eq. 2.20, the final target displacement, δ_t was determined to be 10.2275 in. which corresponds to the base shear of 926.8304 kips. The member forces and deformations determined for the seismic forces corresponding to this base shear. For the baseline MRF frame, the obtained inter-story drifts, column interaction strength ratios, and beam rotations are compared with the same results obtained for the linear static and linear dynamic analysis cases, as shown in Tables 5.15, 5.16, and 5.17, respectively.

Story	Inter-story Drifts (in.)		
	EFP or Linear Static Analysis	**Linear Dynamic Analysis**	**Nonlinear Static Analysis**
	Allowed = 3.12 in.	Allowed = 3.9 in.	Allowed = 3.9 in.
1	2.5322	3.518	2.8458
2	3.5743	4.7252	4.0773
Roof	3.2335	4.0878	3.9805

Table 5.15: Inter-story Drift Comparison for Linear Static, Linear Dynamic, and Nonlinear Static Cases

Column Interaction Strength Check Ratio (<1.0)			
Column No.	**EFP or Linear Static Analysis**	**Linear Dynamic Analysis**	**Nonlinear Static Analysis**
1	1.18	1.25	1.05
2	1.34	1.35	1.06
3	1.33	1.35	1.06
4	1.26	1.25	1.07
5	0.35	0.17	0.46
6	0.65	0.73	0.50
7	1.01	1.0	0.79
8	1.01	1.0	0.79
9	0.74	0.72	0.55
10	0.08	0.04	0.08
11	0.37	0.46	0.28
12	0.64	0.68	0.47
13	0.64	0.68	0.47
14	0.45	0.46	0.31
15	0.04	0.03	0.03

Table 5.16: Column Strength Ratio Comparison for Linear Static, Linear Dynamic, and Nonlinear Static Cases

Beam Plastic Rotations (rad.) (<0.04)			
Beam No.	**EFP or Linear Static Analysis**	**Linear Dynamic Analysis**	**Nonlinear Static Analysis**
16	0.029	0.022	0.030
17	0.023	0.018	0.028
18	0.027	0.022	0.030
19	0.041	0.033	0.037
20	0.029	0.022	0.033
21	0.025	0.019	0.031
22	0.028	0.022	0.033
23	0.037	0.029	0.035
24	0.03	0.023	0.032
25	0.026	0.021	0.030
26	0.027	0.023	0.032
27	0.034	0.027	0.035

Table 5.17: Beam Plastic Rotations Comparison for Linear Static, Linear Dynamic, and Nonlinear Static Cases

From the comparison of results for the three analysis cases, it is observed that the linear dynamic analysis would give the most conservative design, and therefore, the optimization weight/cost is expected to be highest for the linear dynamic case. However, it is difficult to conclude as to what analysis would give the least conservative design because even though the story drifts are least in the linear static case; the column strength ratios are higher than the nonlinear static case. This is because in the equivalent lateral force procedure the columns are designed with an empirical overstrength factor, and so one limitation of using the empirical factor is that the procedure estimates the force and drift responses disproportionately. Whereas, in the advanced analysis cases such as in LD and NLS, both of the responses are commensurate with each other, that is, both strength ratios and drifts are consistently higher or lower than the linear static case.

5.4.3 Optimization

Like the optimization for the linear dynamic case, the standard PSO algorithm was found to be more efficient than the HPSO technique for this case. Therefore, the PSO algorithm was used to optimize the 3-story MRF structure for the nonlinear static case. A code was developed in MATLAB that automated the previously discussed procedures and obtained the final target displacement value at each PSO time step by following an iterative process as shown in Figure 5.10.

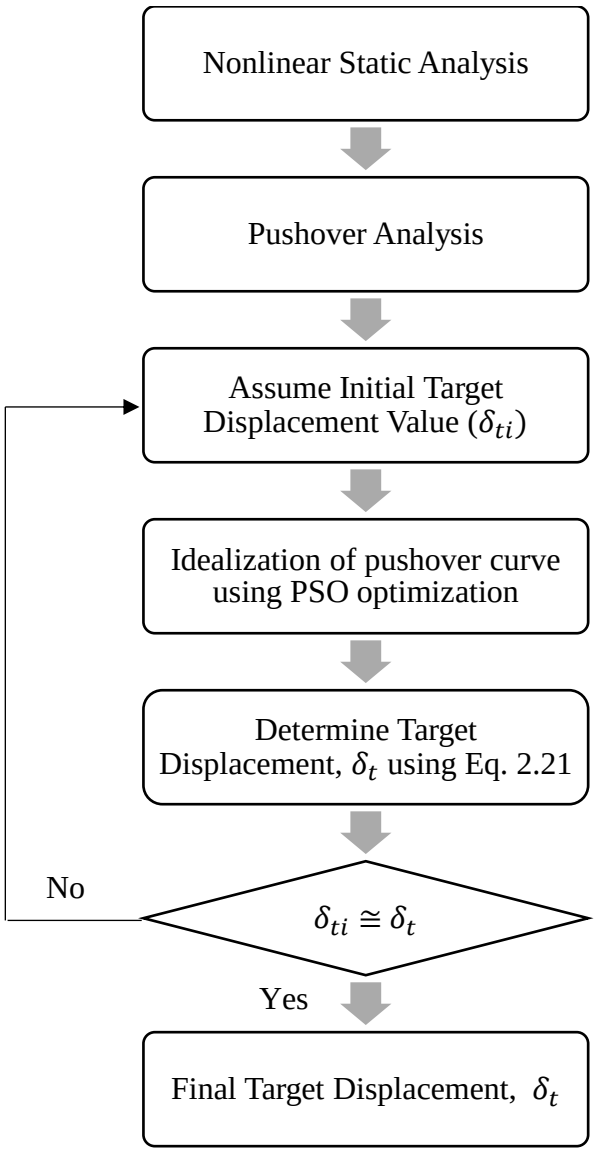

Figure 5.10: Flow chart to obtain Final Target Displacement

Figure 5.11 shows the convergence graph for the seismic design optimization of the of the benchmark building for the nonlinear static case. The optimal weight of the design was obtained to be as 84504 lb.

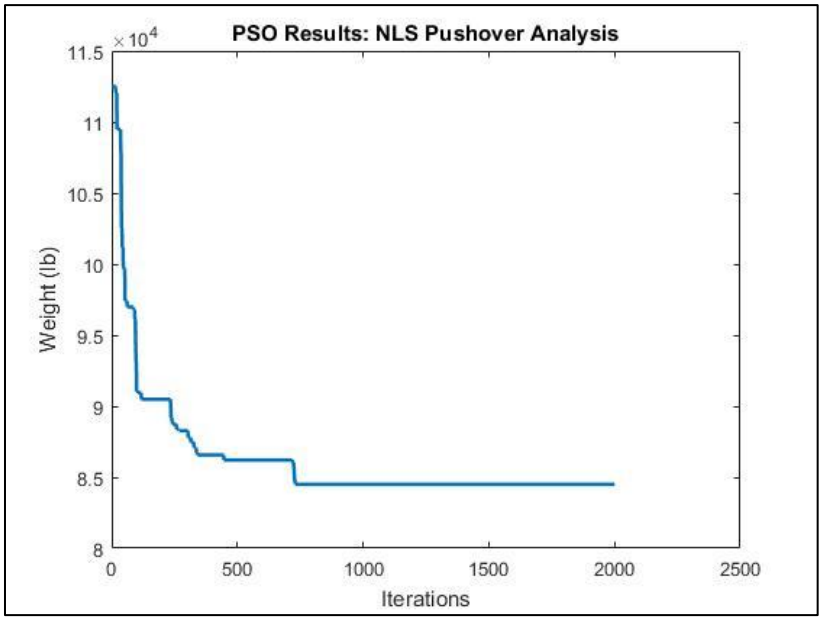

Figure 5.11: PSO Convergence Graph for 3-Story Benchmark Building (Nonlinear Static Case)

5.5 Summary of Results

From Table 5.18 and Table 5.19, it is observed that inter-story drifts govern the optimal designs only for the linear static and linear dynamic analysis; whereas, the column strengths govern the optimal design for all the three analysis methods. Also, the top story experiences the maximum inter-story drift ratio for the linear static and linear dynamic case; whereas, in the nonlinear static case, the maximum inter-story drift is obtained in the second story which is expected, as bottom stories usually experience higher inertial forces due higher story weights. Table 5.20 shows the beam rotations of the optimal frame from each analysis case, and it is evident that beam rotations does not control the optimal weight for any of the three analysis methods. From Table 5.21, it is apparent that the selection of analysis method significantly influences the optimal designs.

Story	Inter-story Drifts (in.)		
	EFP or Linear Static Analysis	**Linear Dynamic Analysis**	**Nonlinear Static Analysis**
	Allowed =3.12 in.	Allowed =3.9 in.	Allowed =3.9 in.
1	2.0772	2.3555	2.1611
2	2.6362	2.8532	**3.7309**
Roof	**3.1178**	**3.8674**	3.6548

Table 5.18: Inter-story Drift Comparison for Optimal Designs

Column Interaction Strength Check Ratio (<1.0)			
Column No.	**EFP or Linear Static Analysis**	**Linear Dynamic Analysis**	**Nonlinear Static Analysis**
1	0.9045	0.9647	0.9871
2	**0.9942**	0.9982	0.9986
3	0.9927	**0.9983**	0.9981
4	0.9837	0.9625	**0.9999**
5	0.9020	0.7685	0.8625
6	0.6241	0.6573	0.6517
7	0.7232	0.7228	0.8842
8	0.7189	0.7223	0.8840
9	0.6982	0.6613	0.6966
10	0.5649	0.4861	0.5138
11	0.5437	0.6972	0.4088
12	0.6390	0.7851	0.5991
13	0.6359	0.7847	0.5989
14	0.6054	0.7050	0.4346
15	0.2558	0.2219	0.2291

Table 5.19: Column Strength Ratio Comparison for Optimal Design

Beam Plastic Rotations (rad.) (<0.04)			
Beam No.	**EFP or Linear Static Analysis**	**Linear Dynamic Analysis**	**Nonlinear Static Analysis**
16	0.013	0.0115	0.0230
17	0.013	0.0110	0.0203
18	0.013	0.0115	0.0228
19	0.027	0.0202	0.0299
20	0.019	0.0111	0.0323
21	0.019	0.0106	0.0322
22	0.019	0.0111	0.0322
23	0.023	0.0214	0.0322
24	0.012	0.0294	0.0252
25	0.011	0.0292	0.0231
26	0.011	0.0293	0.0251
27	0.020	0.0292	0.0307

Table 5.20: Beam Plastic Rotations Comparison for Optimal Designs

Optimal Designs Comparison				
Group	**Member**	**EFP or Linear Static Analysis**	**Linear Dynamic Analysis**	**Nonlinear Static Analysis**
1	Column	W14 X 257	W14 X 283	W14 X 283
2	Column	W14 X 426	W14 X 455	W14 X 370
3	Column (Weak Axis)	W14 X 30	W14 X 22	W14 X 30
4	Beam	W40 X 149	W40 X 167	W40 X 149
5	Truss	W18 X 35	W16 X 40	W16 X 31
6	Beam	W36 X 182	W40 X 183	W30 X 90
7	Beam	W21 X 44	W14 X 74	W30 X 90
	Optimal Weight (lb)	**91344**	**100182**	**84504**

Table 5.21: Comparison of Optimal Designs for 3-story Benchmark Building

Chapter 6: Performance-Based Design Optimization of 3-Story MRF

6.1 Introduction

In this chapter, the performance-based design (PBD) optimization of the 3-story MRF is performed for the nonlinear static (pushover analysis) case due to its ability to determine the nonlinear response of structures under high earthquake intensities. The four building performance levels of Operational Level (OL), Immediate Occupancy (IO), Life Safety (LS), and Collapse Prevention (CP) can be combined with three hazard levels of Frequent Earthquake, Design Earthquake (DE), and Maximum Considered Earthquake (MCE), as per Figure 5.14 [69]. Since the benchmark office building corresponds to the Risk Category II, the objectives for its performance-based design of the 3-story MRF will include three performance levels- IO, LS, and CP.

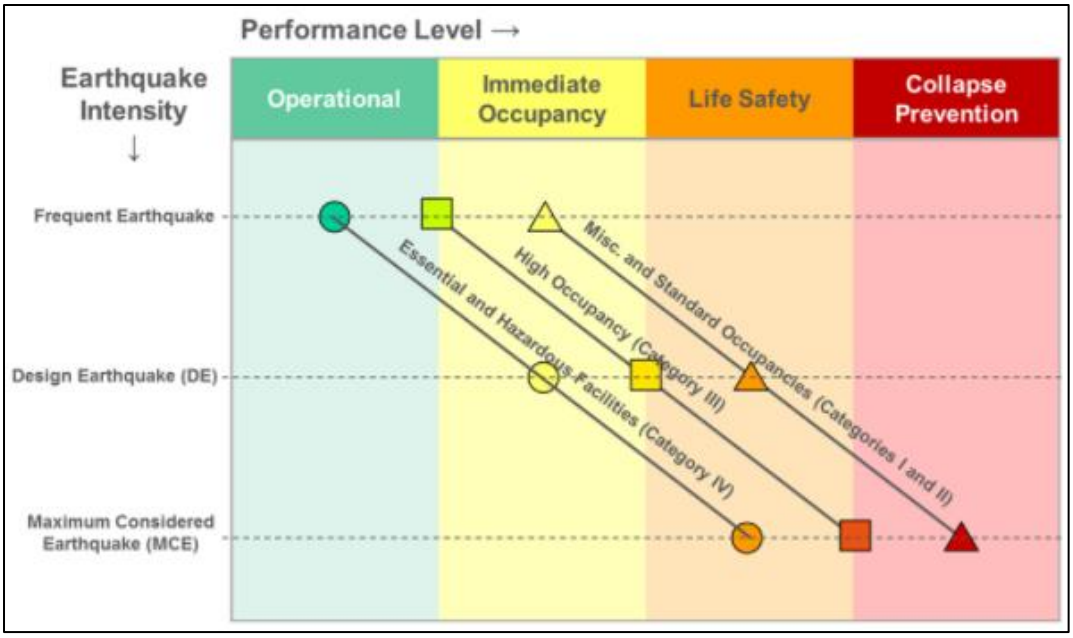

Figure 6.1: Performance-Based Design Objectives [70]

6.2 PBD Optimization

The PSO algorithm was used for the performance-based design optimization of the 3-story benchmark building. A code was developed in MATLAB that automated the previously discussed nonlinear static procedures, and conformed to the acceptance criteria specified in the performance-based codes of FEMA-356/ASCE-41 (Section 2.3.6). The selected performance-based design criteria are summarized in Table 6.1. The spectral acceleration parameters for the probabilistic seismic hazard levels shown in Table 6.1 were obtained from the USGS website. At every optimization time step, three separate analyses were performed to obtain target displacements, member forces and drifts for the seismic forces corresponding to the three earthquake levels.

Earthquake Levels	**Probability of Exceedance**	$S_s(g)$	$S_1(g)$	**Performance Level (Objective)**	**Target Drift Ratios**
Frequent Level	20% in 50 years	0.988	0.544	IO (Enhanced)	0.7%
Design Earthquake	10% in 50 years	1.622	0.853	LS (Basic Safety)	2.5 %
Maximum Considered Earthquake	2% in 50 years	2.433	1.279	CP (Limited)	5%

Table 6.1: FEMA 356/ASCE 41 Performance-Based Design Criteria

Figure 6.2 shows the convergence graph for the PBD optimization of the of the benchmark building for the nonlinear static case. The optimal weight of the frame was obtained to be as 91926 lb. which shows that the optimal weight for the Enhanced Objective is 8.78% higher than the optimal weight for the Life Safety Objective (84504 lb.). This corroborates with the Figure 2.6 showing the surface plots of the relative costs for different performance objectives, i.e., surface "e" is higher than "c". Tables 6.2 and 6.3 shows the comparison of the inter-story drifts and column rotations, respectively, for the three performance levels for the optimal frame. From Table 6.2 and Figure 6.3, it is evident that the immediate occupancy governs among the three performance levels,

which validates the definition of the Enhanced objective provided in Table 2.5. Table 6.4 shows the comparison of the optimal designs for the Life Safety Objective (Section 5.4.3) and the Enhanced Objective for the nonlinear static cases.

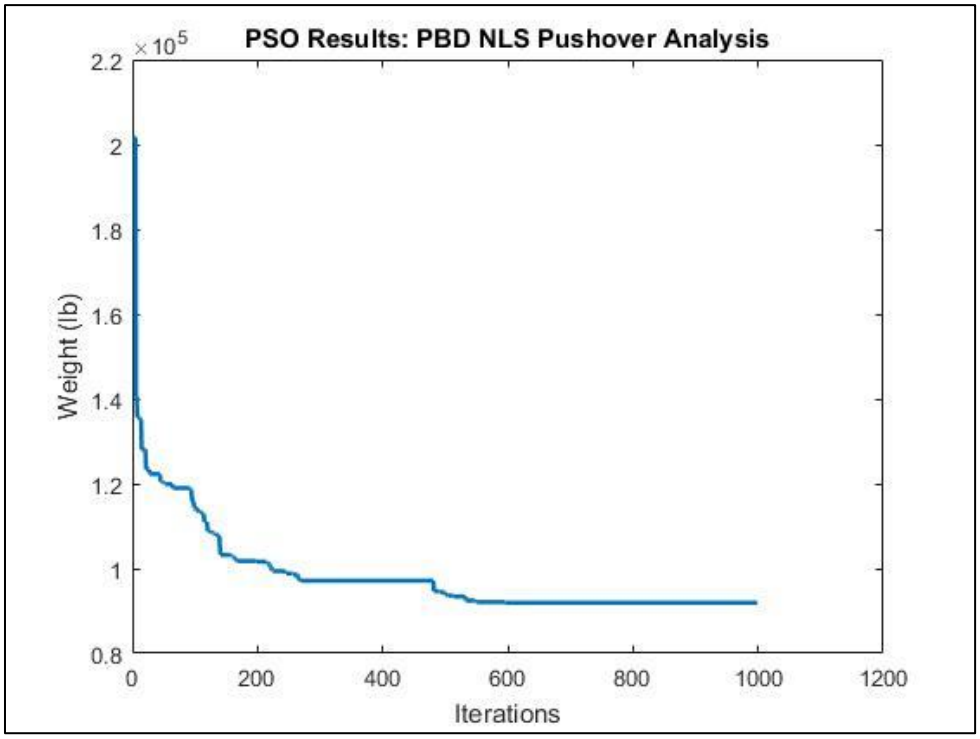

Figure 6.2: PSO Convergence Graph for PBD of 3-Story Benchmark Building for NLS analysis

Immediate Occupancy			**Life Safety**			**Collapse Prevention**		
Δ (in.)	Allowed	Check	Δ (in.)	Allowed	Check	Δ (in.)	Allowed	Check
0.9679	1.09	OK	3.6852	3.9	OK	5.3801	7.8	OK
1.0612	1.09	OK	3.2878	3.9	OK	4.8497	7.8	OK
1.0073	1.09	OK	2.3997	3.9	OK	3.3048	7.8	OK

Table 6.2: Inter-Story Drift Check for PBD Optimal Design for NLS analysis

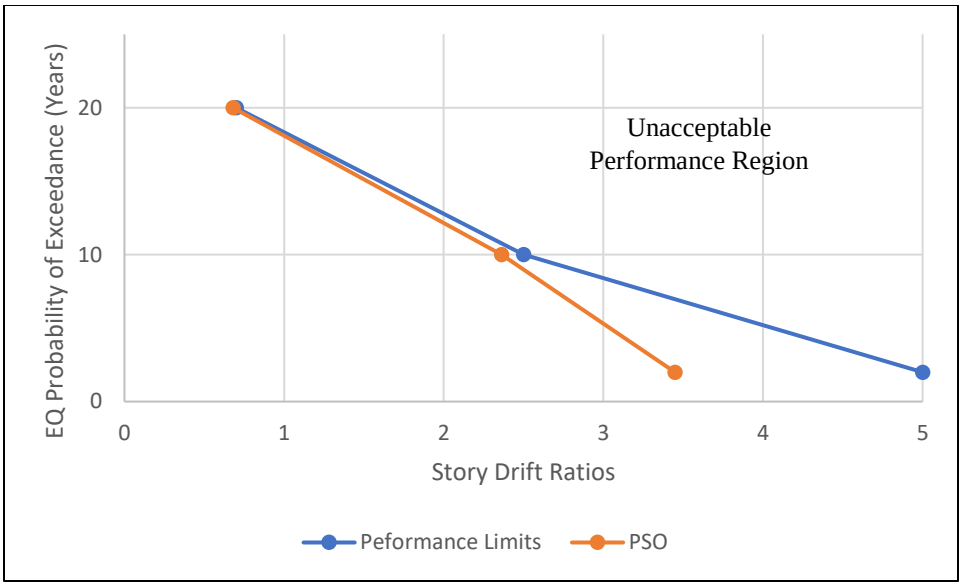

Figure 6.3: Inter-Story Drift Ratios Graph for PBD Optimal Design for NLS analysis

Col. No.	Immediate Occupancy			Life Safety			Collapse Prevention		
	Column Rot. (rad.)	Allowed	Check	Column Rot. (rad.)	Allowed	Check	Column Rot. (rad.)	Allowed	Check
1	0.0047	0.0067	OK	0.0202	0.0388	OK	0.0303	0.0514	OK
2	0.0015	0.0064	OK	0.0019	0.0374	OK	0.0021	0.0496	OK
3	0.0015	0.0069	OK	0.0020	0.0426	OK	0.0020	0.0572	OK
4	0.0045	0.0061	OK	0.0199	0.0355	OK	0.0296	0.0469	OK
5	0.0082	0.0154	OK	0.0295	0.0925	OK	0.0433	0.1233	OK
6	0.0034	0.0068	OK	0.0112	0.0401	OK	0.0163	0.0532	OK
7	0.0011	0.0068	OK	0.0014	0.0400	OK	0.0015	0.0532	OK
8	0.0011	0.0070	OK	0.0013	0.0425	OK	0.0014	0.0568	OK
9	0.0033	0.0064	OK	0.0110	0.0379	OK	0.0161	0.0503	OK
10	**0.0063**	0.0064	OK	0.0162	0.0382	OK	0.0233	0.0510	OK
11	0.0065	0.0068	OK	0.0151	0.0412	OK	0.0211	0.0549	OK
12	0.0044	0.0071	OK	0.0122	0.0424	OK	0.0178	0.0566	OK
13	0.0044	0.0071	OK	0.0122	0.0424	OK	0.0177	0.0566	OK
14	0.0061	0.0067	OK	0.0151	0.0402	OK	0.0210	0.0536	OK
15	0.0066	0.0205	OK	0.0150	0.1232	OK	0.0201	0.1643	OK

Table 6.3: Column Rotations Check for PBD Optimal Design for NLS analysis

Optimal Design Comparison			
Group	**Member**	**Basic (Life Safety) Objective**	**PBD (Enhanced) Objective**
1	Column	W14 X 283	W14 X 311
2	Column	W14 X 370	W14 X 211
3	Column (Weak Axis)	W14 X 30	W14 X 30
4	Beam	W40 X 149	W40 X 215
5	Truss	W16 X 31	W18 X 35
6	Beam	W30 X 90	W44 X 230
7	Beam	W30 X 90	W24 X 76
	Weight (lb)	**84504**	**91926**

Table 6.4: Comparison of Optimal PBD for Nonlinear Static Analysis

Chapter 7: Sensitivity Analysis

7.1 Introduction

This chapter investigates the sensitivity of the two design parameters, fundamental period, T and the effective length factor, K, to the optimization of the benchmark frame for the ASCE 7-10 equivalent lateral force procedure. This was based on the finding that the codes ASCE 7-10 and FEMA 356 either did not agree or did not provide guidelines, on the use of the two parameters in their seismic design procedures. Thus, the optimization results are compared by assuming different values for each of these parameters.

7.1 Fundamental Period Determination

As discussed in Section 2.3.3, ASCE 7-10's equivalent lateral force procedure requires using an upper limit for the period determination. On the other hand, FEMA-356 permits using a computed period from modal analysis. Therefore, to compare of the influence of using the upper period instead of the computed period, the optimization was performed using the equivalent lateral force procedure with computed period, and the obtained results were compared with the optimization results obtained earlier in Section 5.2.2 where the upper period was used. Figure 7.1 shows the convergence graph of the optimization of the benchmark frame using EFP with computed period. The optimal weight was obtained as 90930 lb. which is very close to the optimal weight of 91344 lb obtained in the earlier case with a difference of only 0.5%. Tables 7.1 and 7.2 the comparison of inter-story drifts and column strength ratios, for the two cases. From the results comparison, it is observed that drift values for the computer period case are farther from the upper limit of 3.12 in. as compared to the previous case. However, the optimal costs still end being close because the column strength controls in both cases, as shown in Table 6.4

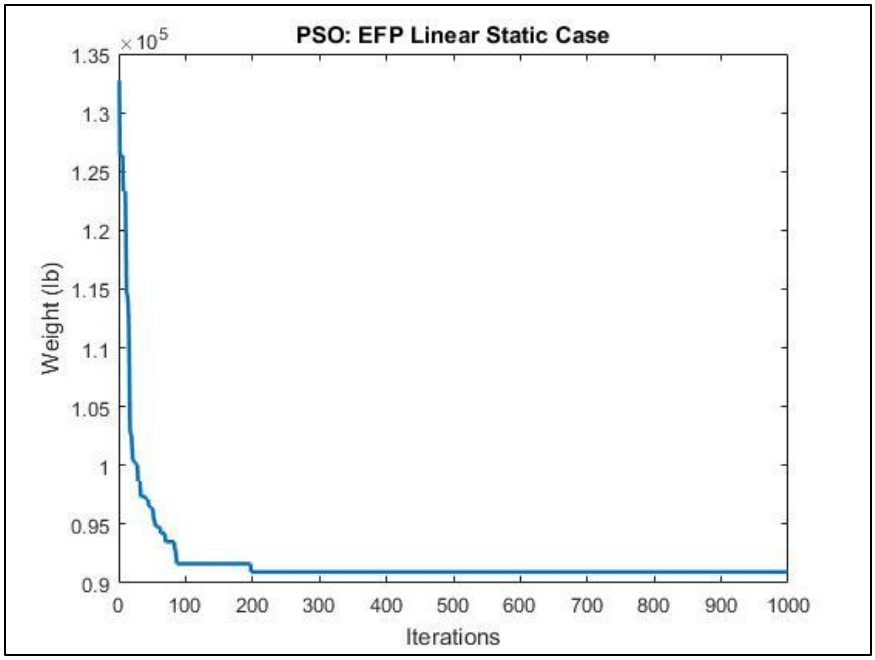

Figure 7.1: PSO Convergence Graph for Equivalent Lateral Force Procedure with Computed Period

Story	Story Drifts (in.)	
	(Δa) = 3.12 in.	
	EFP with Upper Period Limit	**EFP with Computed Period**
1	2.0772	2.4269
2	2.6362	2.6723
Roof	**3.1178**	3.0776

Table 7.1: Optimal Frame's Inter-Story Drifts Comparison for Upper Period Vs. Computed Period for EFP (LS) analysis

Column Strength Check Ratio		
Column No.	**EFP with Upper Period Limit**	**EFP with Computed Period**
1	0.9045	0.8905
2	**0.9942**	**0.9995**
3	0.9927	0.9941
4	0.9837	0.9806
5	0.902	0.2872
6	0.6241	0.6742
7	0.7232	0.8445
8	0.7189	0.8370
9	0.6982	0.7520
10	0.5649	0.0912
11	0.5437	0.5843
12	0.639	0.7174
13	0.6359	0.7138
14	0.6054	0.6462
15	0.2558	0.0469

Table 7.2: Optimal Frame's Column Strength Ratio Comparison for Upper Period Vs. Computed Period

7.2 Effective Length Factor (K)

As discussed in Section 2.2.1, the AISC manual recommends either of the two methods for determining the effective length factor- Alternate Design Method or Direct Design Method. Whereas, the AISC Seismic Provisions recommends using $K = 1$ based on the recognition that in the moment resisting frames, column bending moments would largest at column ends, resulting in reverse curvature in the column, therefore the assumption of taking K as 1.0 would be conservative. The seismic procedures of ASCE 7-10 does not provide guidelines for determining the effective length factor (K), but the FEMA-356 allows K to be taken as 1.0 for seismic design procedures.

Thus, to test the impact of these incongruities on the optimal design of the MRF frame, the optimization is performed again for the equivalent lateral force procedure using the Direct Design Method as opposed to the previous optimization case of Section 5.2.2 where K was taken as unity. Figure 7.2 shows the convergence graph of the optimization of the benchmark frame using EFP with AISC Direct Design Method. The optimal weight was obtained as 99633 lb. which is significantly higher, i.e., 9% than the optimal weight of 91344 lb. obtained in the earlier case. The difference is expected because the Direct Design Method requires the member stiffnesses to be reduced by 20% along with additional lateral notional loads. Therefore, the method results in an over conservative design. Tables 7.3 and 7.4 shows the comparison of inter-story drifts and column strength ratios, for the two cases. From the results comparison, it is observed that drift values for the computer period case are far from the upper limit of 3.12 in., and thus it is apparent that the strength design controls when AISC Direct Design Method is used.

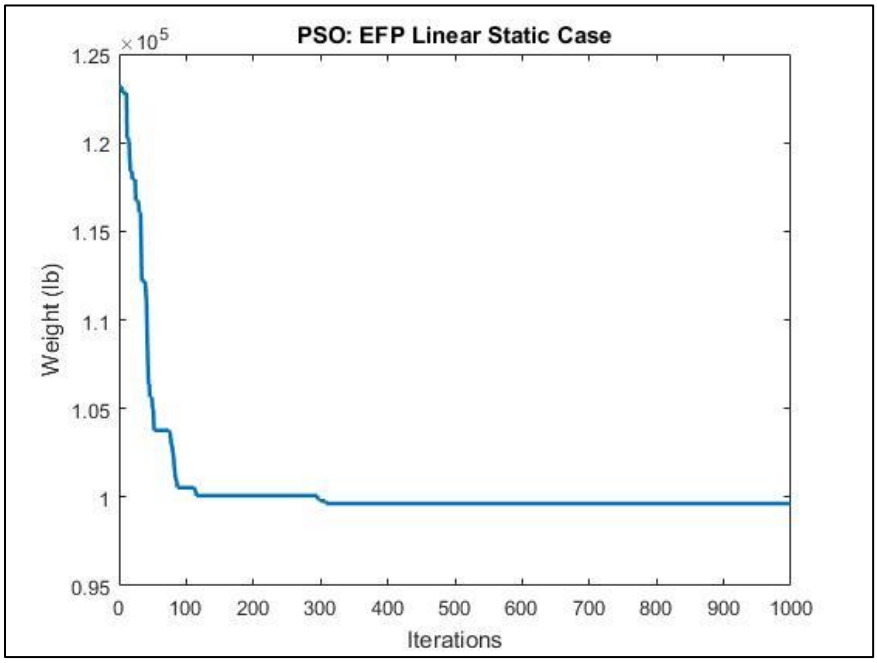

Figure 7.2: PSO Convergence Graph for Equivalent Lateral Force Procedure with AISC Direct Design Method

Story	Story Drifts (in.)	
	(Δa) = 3.12 in.	
	EFP with K=1.0	EFP with AISC Direct Design Method
1	2.0772	2.1195
2	2.6362	2.4204
Roof	**3.1178**	2.9401

Table 7.3: Optimal Frame's Inter-Story Drifts Comparison for AISC Direct Design Method

Column Strength Check Ratio		
Column No.	EFP with K=1.0	EFP with AISC Direct Design Method
1	0.9045	0.8919
2	**0.9942**	**0.9977**
3	0.9927	0.9917
4	0.9837	0.9646
5	0.902	0.2954
6	0.6241	0.6434
7	0.7232	0.8304
8	0.7189	0.8236
9	0.6982	0.7082
10	0.5649	0.0867
11	0.5437	0.5830
12	0.639	0.7273
13	0.6359	0.7247
14	0.6054	0.6354
15	0.2558	0.0536

Table 7.4: Optimal Frame's Column Strength Ratio Comparison for AISC Direct Design Method

Chapter 8: Summary and Conclusions

8.1 Summary

The objective of this study was to create a framework that combines metaheuristic algorithms with state-of-the-art finite element analysis for optimal seismic design of structures; enabling the consideration of advanced analysis procedures in the optimization. An existing office building comprising of a three-story steel moment-resisting frame was selected as a benchmark structure for this purpose. The optimization of the structure was performed for linear static, linear dynamic, and nonlinear static analysis cases. The framework enabled a study across analysis cases with regard to the resulting optimal seismic design. In addition, the influence of design decisions and sensitivity to parameter selection is assessed using the optimization framework.

Principles of current seismic design procedures were presented, followed by a theoretical background of the seismic design codes of ASCE 7-10 and FEMA-356. The PSO algorithm was developed in MATLAB and the code was validated through two numerical examples, which included optimization of a 10-bar planar truss and a six-story rigid steel frame.

The finite element software OpenSees was utilized to model and analyze linear, nonlinear and dynamic response of the structure, for which an interface between MATLAB and OpenSees was created. Therefore, a code was developed in MATLAB that performed the analyses using OpenSees and conformed to the seismic design criteria specified in the design codes. The seismic design optimization was performed for the three analysis cases separately, followed by the performance-based design optimization of the benchmark building using nonlinear static analysis.

Lastly, sensitivity of the two design parameters including fundamental period (T) and effective length factor (K) was evaluated by comparing the optimal designs with changed

parameters against the original optimization results. The optimization results and the computational time for each analysis case is summarized in Table 8.1.

Optimization Case	**Algorithm**	**Swarm Size**	**Computation Time* (sec) Per Iteration**	**Optimum Weight (lb)**	**Governing Constraints****
Linear Static	HPSO	25	127.8309	91344	Inter-story drifts, Column strength
Linear Dynamic	PSO	25	3633.9856	100182	Inter-story drifts, Column strength
Nonlinear Static	PSO	25	197.64	84504	Column strength
Performance-based Design	PSO	25	241.3598	91926	Inter-story drift (Immediate Occupancy)
*	The computation times are based on Intel i7 CPU @ 3.40 GHz Clock Speed and 8.00 GB Memory.				
**	The governing constraints are picked based on the constraint which was closest to the upper bound value.				

Table 8.1: Optimization Results Summary

8.2 Conclusions

The metaheuristic algorithms including PSO and HPSO were successfully applied to the seismic and performance-based design of the three-story moment resisting frame for equivalent lateral force, linear response time-history, and nonlinear static analysis procedures, by utilizing an interface between MATLAB and OpenSees. Among the three analysis cases, the lowest and the highest optimum weights of 84505 lb and 100182 lb were obtained in the nonlinear static case and linear dynamic case, respectively. Based on the optimization results obtained from different analysis procedures, following conclusions were made:

ASCE 7-10 Equivalent Lateral Force Procedure (Linear Static Case):

- The optimal weight was obtained as 91344 lb in the linear static case and was the second highest among the three analysis cases. The optimum design was governed by inter-story drifts and column strength.
- The optimization time was lowest in the linear static case (see Table 8.1), and since this analysis uses a linear elastic model, the analysis is relatively simpler to perform as compared to the other analysis procedures.
- Since the analysis procedure relies on the linear elastic analysis, the results are not very accurate. To predict the actual nonlinear response, the code scales the results by making the use of empirical factors such as Ω_o, C_d, etc. which leads to more conservative results and up to 8% higher optimum design cost.
- The base shear calculation depends on the fundamental period; therefore, the period must be computed at every iteration. Because the code requires member forces and drifts to be determined using different fundamental period values (computed period and an upper bound value using approximate period), two separate analyses had to be performed. However, from the sensitivity analysis, it was determined that if both member forces and drifts were determined using the computed period value, the optimization results were very close with only 0.5% of difference. So, it is recommended to only use the computed period value to save additional steps and computation time.
- There are no guidelines regarding the effective length factor in the ASCE 7-10 codes, and different values of the factor can significantly affect the optimization results as noted in the proceeding conclusions.

ASCE 7-10 Linear Response Time History Procedure (Linear Dynamic Case):

- The optimal weight was 100182 lb and was heaviest among all the analysis cases, and the governing design constraints were both inter-story drifts and column strengths.
- Since the analysis considers the dynamic response of the structure, the results are more accurate. However, the response depends on the suite of ground motions considered, therefore the optimization results could vary significantly.
- To consider the mean response from the suite of ground motions, at least seven ground motion records must be considered, which makes the optimization highly computationally intensive- resulting in more than an hour per iteration (see Table 8.1).
- The code requires scaling of the ground motions values to obtain suitable mean response spectrum that matches with the general design response spectrum. The scale factors are obtained using guess and check approach and can be very difficult to automate for the optimization.
- Between linear static and linear dynamic procedures, the former is recommended for the seismic design optimization (provided the structural configurations are similar) based on the comparison of their computational times, conservativeness of results, and simplicity.

FEMA-356 Nonlinear Static Procedure (Nonlinear Static Case):

- The optimal weight was lightest among all the analyses cases, which was obtained as 84054 lb. The optimization was found to be more governed by column strengths than drift ratios.
- The analysis incorporates the nonlinear behavior of the individual members, and therefore it accurately predicts the seismic demand and is suitable for the performance-based design of the structure.

- Although, the concentrated plasticity model is comparatively more computationally efficient; it is inefficient to be considered in the optimization because the concentrated plasticity model requires moment-curvature relationship of individual members, which are based on various experimental results and can be difficult to simulate for optimization.
- The analysis procedure includes iterative graphical procedure to obtain an idealized pushover curve. Additionally, an iterative procedure had to be performed to obtain the final target displacement value. This makes the analysis procedure to be complex and time consuming.

Performance-Based Design (Nonlinear Static Case):

- The Immediate Occupancy or the Enhanced performance objective governs the performance-based optimization with inter-story drift as the governing constraint.
- The performance-based design optimization for the nonlinear static case would be more accurate than performance-based design optimization for the linear static or linear dynamic cases.
- Since three target building performance levels must be considered in the design, the nonlinear static procedures were performed for each of the three performance levels making the optimization very computationally intensive.
- It is observed that the optimal weight for the performance-based design is only 0.64% heavier than that of the linear static case (designed for basic Life Safety), therefore the performance-based design optimization is recommended over the linear static case because the former not only meets the basic life safety or collapse prevention criteria, but also controls structural and nonstructural damages for nearly the same amount of design cost.

AISC Effective Length Factor (K):

- The use of effective length factor required for column designs significantly impacts the optimization results. By using AISC Direct Design Method, the optimum weight was found to be 9% heavier as compared to the design optimization where *K* was assumed as unity.
- The AISC Direct Design Method results in conservative design, and if this method is used for drift computation as well, it will lead to even more conservative and costlier design.

8.3 Future Work

1. Although PSO is an effective technique, there are other metaheuristic algorithms that have been proven to be more robust, for which the seismic design optimization can be performed. Additionally, multiple-objective seismic design optimization can be performed using metaheuristic algorithms that can consider other design variables such as construction costs, labor utilization, etc.
2. To create an optimization framework that would be more readily accepted by the design community, a more familiar finite element software can be integrated. SAP2000 could be used for performing the structural design optimization for the above analysis procedures by taking an advantage of its open application programming interface feature.
3. The application can be extended to obtain optimal weights for other seismic-force resisting frames such as concentrically braced frames and eccentrically braced frames, and include 3-D analysis of the structure.
4. In FEMA 440 document, the improvement of the nonlinear static procedures has been presented which would be desirable to be used for the performance-based design optimization.

APPENDIX A

Seismic Force-Resisting System	ASCE 7 Section Where Detailing Requirements Are Specified	Response Modification Coefficient, R[a]	Overstrength Factor, Ω_0[g]	Deflection Amplification Factor, C_d[b]	Structural System Limitations Including Structural Height, h_n (ft) Limits[c] Seismic Design Category				
					B	C	D[d]	E[d]	F[e]
C. MOMENT-RESISTING FRAME SYSTEMS									
1. Steel special moment frames	14.1 and 12.2.5.5	8	3	5½	NL	NL	NL	NL	NL
2. Steel special truss moment frames	14.1	7	3	5½	NL	NL	160	100	NP
3. Steel intermediate moment frames	12.2.5.7 and 14.1	4½	3	4	NL	NL	35[h]	NP[h]	NP[h]
4. Steel ordinary moment frames	12.2.5.6 and 14.1	3½	3	3	NL	NL	NP[i]	NP[i]	NP[i]
5. Special reinforced concrete moment frames[n]	12.2.5.5 and 14.2	8	3	5½	NL	NL	NL	NL	NL
6. Intermediate reinforced concrete moment frames	14.2	5	3	4½	NL	NL	NP	NP	NP
7. Ordinary reinforced concrete moment frames	14.2	3	3	2½	NL	NP	NP	NP	NP
8. Steel and concrete composite special moment frames	12.2.5.5 and 14.3	8	3	5½	NL	NL	NL	NL	NL
9. Steel and concrete composite intermediate moment frames	14.3	5	3	4½	NL	NL	NP	NP	NP
10. Steel and concrete composite partially restrained moment frames	14.3	6	3	5½	160	160	100	NP	NP
11. Steel and concrete composite ordinary moment frames	14.3	3	3	2½	NL	NP	NP	NP	NP
12. Cold-formed steel—special bolted moment frame[p]	14.1	3½	3[o]	3½	35	35	35	35	35

Design Coefficients and Factors for Seismic Force-Resisting Systems [71].

APPENDIX B

Table 5-6 Modeling Parameters and Acceptance Criteria for Nonlinear Procedures—Structural Steel Components

	Modeling Parameters			Acceptance Criteria				
	Plastic Rotation Angle, Radians		Residual Strength Ratio	Plastic Rotation Angle, Radians				
					Primary		Secondary	
Component/Action	a	b	c	IO	LS	CP	LS	CP
Beams—flexure								
a. $\frac{b_f}{2t_f} \le \frac{52}{\sqrt{F_{ye}}}$ and $\frac{h}{t_w} \le \frac{418}{\sqrt{F_{ye}}}$	$9\theta_y$	$11\theta_y$	0.6	$1\theta_y$	$6\theta_y$	$8\theta_y$	$9\theta_y$	$11\theta_y$
b. $\frac{b_f}{2t_f} \ge \frac{65}{\sqrt{F_{ye}}}$ or $\frac{h}{t_w} \ge \frac{640}{\sqrt{F_{ye}}}$	$4\theta_y$	$6\theta_y$	0.2	$0.25\theta_y$	$2\theta_y$	$3\theta_y$	$3\theta_y$	$4\theta_y$
c. Other	Linear interpolation between the values on lines a and b for both flange slenderness (first term) and web slenderness (second term) shall be performed, and the lowest resulting value shall be used							
Columns—flexure [2, 7]								
For $P/P_{CL} < 0.20$								
a. $\frac{bf}{2t_f} \le \frac{52}{\sqrt{F_{ye}}}$ and $\frac{h}{t_w} \le \frac{300}{\sqrt{F_{ye}}}$	$9\theta_y$	$11\theta_y$	0.6	$1\theta_y$	$6\theta_y$	$8\theta_y$	$9\theta_y$	$11\theta_y$
b. $d\ \frac{bf}{2t_f} \ge \frac{65}{\sqrt{F_{ye}}}$ or $\frac{h}{t_w} \ge \frac{460}{\sqrt{F_{ye}}}$	$4\theta_y$	$6\theta_y$	0.2	$0.25\theta_y$	$2\theta_y$	$3\theta_y$	$3\theta_y$	$4\theta_y$
c. Other	Linear interpolation between the values on lines a and b for both flange slenderness (first term) and web slenderness (second term) shall be performed, and the lowest resulting value shall be used							

Acceptance Criteria for Nonlinear Procedures [72].

APPENDIX C

Table 5-2 Default Lower-Bound Material Strengths[1]

Properties based on ASTM and AISC Structural Steel Specification Stresses

Date	Specification	Remarks	Tensile Strength[2], ksi	Yield Strength[2], ksi
1900	ASTM, A9	Rivet Steel	50	30
	Buildings	Medium Steel	60	35
1901–1908	ASTM, A9	Rivet Steel	50	25
	Buildings	Medium Steel	60	30
1909–1923	ASTM, A9	Structural Steel	55	28
	Buildings	Rivet Steel	46	23
1924–1931	ASTM, A7	Structural Steel	55	30
		Rivet Steel	46	25
	ASTM, A9	Structural Steel	55	30
		Rivet Steel	46	25
1932	ASTM, A140-32T issued as a tentative revision to ASTM, A9 (Buildings)	Plates, Shapes, Bars	60	33
		Eyebar flats unannealed	67	36
1933	ASTM, A140-32T discontinued and ASTM, A9 (Buildings) revised Oct. 30, 1933	Structural Steel	55	30
	ASTM, A9 tentatively revised to ASTM, A9-33T (Buildings)	Structural Steel	60	33
	ASTM, A141-32T adopted as a standard	Rivet Steel	52	28
1934 on	ASTM, A9	Structural Steel	60	33
	ASTM, A141	Rivet Steel	52	28
1961 – 1990	ASTM, A36/A36M-00	Structural Steel		
	Group 1		62	44
	Group 2		59	41
	Group 3		60	39
	Group 4		62	37
	Group 5		70	41
1961 on	ASTM, A572, Grade 50	Structural Steel		
	Group 1		65	50
	Group 2		66	50
	Group 3		68	51
	Group 4		72	50
	Group 5		77	50
1990 on	A36/A36M-00 & Dual Grade	Structural Steel		
	Group 1		66	49
	Group 2		67	50
	Group 3		70	52
	Group 4		70	49

1. Lower-bound values for material prior to 1960 are based on minimum specified values. Lower-bound values for material after 1960 are mean minus one standard deviation values from statistical data.
2. The indicated values are representative of material extracted from the flanges of wide flange shapes.

Table 5-3 Factors to Translate Lower-Bound Steel Properties to Expected-Strength Steel Properties

Property	Year	Specification	Factor
Tensile Strength	Prior to 1961		1.10
Yield Strength	Prior to 1961		1.10
Tensile Strength	1961-1990	ASTM A36/A36M-00	1.10
	1961-present	ASTM A572/A572M-89, Group 1	1.10
		ASTM A572/A572M-89, Group 2	1.10
		ASTM A572/A572M-89, Group 3	1.05
		ASTM A572/A572M-89, Group 4	1.05
		ASTM A572/A572M-89, Group 5	1.05
	1990-present	ASTM A36/A36M-00 & Dual Grade, Group 1	1.05
		ASTM A36/A36M-00 & Dual Grade, Group 2	1.05
		ASTM A36/A36M-00 & Dual Grade, Group 3	1.05
		ASTM A36/A36M-00 & Dual Grade, Group 4	1.05
Yield Strength	1961-1990	ASTM A36/A36M-00	1.10
	1961-present	ASTM A572/A572M-89, Group 1	1.10
		ASTM A572/A572M-89, Group 2	1.10
		ASTM A572/A572M-89, Group 3	1.05
		ASTM A572/A572M-89, Group 4	1.10
		ASTM A572/A572M-89, Group 5	1.05
	1990-present	ASTM A36/A36M-00, Rolled Shapes	1.50
		ASTM A36/A36M-00, Plates	1.10
		Dual Grade, Group 1	1.05
		Dual Grade, Group 2	1.10
		Dual Grade, Group 3	1.05
		Dual Grade, Group 4	1.05
Tensile Strength	All	Not Listed [1]	1.10
Yield Strength	All	Not Listed [1]	1.10

1. For materials not conforming to one of the listed specifications.

Lower Bound Material Strengths [73].

REFERENCES

1. Statista. (2017). *Most significant natural disasters worldwide by death toll up to 2016*. Retrieved from https://www.statista.com/statistics/268029/natural-disasters-by-death-toll-since-1980/

2. Zhang, Bo. (2013). *Top Most Expensive Natural Disasters in History*. Retrieved from https://www.accuweather.com/en/weather-news/top-5-most-expensive-natural-d/47459

3. Meyersohn, N. (2017). *The costliest natural disasters in U.S. history.* Retrieved from http://money.cnn.com/2017/09/11/news/costliest-natural-disasters/index.html

4. Yang, X. (2011). Metaheuristic optimization. Cambridge University, UK. Scholarpedia, 6(8):11472. DOI: http://www.scholarpedia.org/article/Metaheuristic Optimization

5. Blum, C. and Roli, A. (2003). Metaheuristics in combinatorial optimization: Overview and conceptual comparison. *ACM Computing Surveys (CSUR)*, 0360-0300. DOI: http://dx.doi.org/10.1145/937503.937505

6. Gandomi, A.H., Yang, X., Talatahari, S., and Alavi, A.H. (2013). Metaheuristic Applications in Structures and Infrastructures. London, U.K. Elsevier.

7. Goldberg, D.E., and Samtami, M.P. (1986). Engineering optimization via genertic algorithms. *Proc., 9th Conf. on Electronic Comput.* New York, NY. ASCE: 471-482.

8. Lin, C-Y., Hajela, P. (1994). Design optimization with advanced genetic search strategies. *J Adv Eng Softw*: 21:179-189.

9. May, S.A. and Balling, R.J. (1992). A filtered simulated annealing strategy for discrete optimization of 3D steel frameworks. DOI: https://doi.org/10.1007/BF01742735

10. Bland, J.A. (2007). Optimal structural design by ant colony optimization. Taylor & Francis. DOI: https://doi.org/10.1007/BF01742735

11. Lee, Kang and Geem, Zong Woo. (2004). A new structural optimization method based on the harmony search algorithm. Computers & Structures. 82. 781-798. DOI: 10.1016/j.compstruc.2004.01.002

12. Kaveh, A. and Talatahari, S. (2007). A discrete particle swarm ant colony optimization for design of steel frames. *Asian J. Civil. Eng.*, 9(6), 563-575.

13. Yang, X.S. and Deb, S. (2009). Cuckoo search via Levy flights. *Proceedings of World Congress on Nature and Biologically Inspired Computing*. IEEE Publications, USA, pp. 210-214. DOI: 10.1109/NABIC.2009.5393690

14. Kaveh, A. and Bakshpoori, T. (2012). Optimum design of steel frames using cuckoo search algorithm with Levy flights. *Struct. Design Tall Spec. Build.* DOI: 10.1002/tal.754

15. Kaveh, A., Azar, B. Farahmand, Hadidi, A., Sorochi, F. Rezazadeh, and Talatahari, S. (2009). Performance-based seismic design of steel frames using ant colony optimization. *Journal of Constructional Steel Research.* DOI: https://doi.org/10.1016/j.jcsr.2009.11.006

16. Gholizadeh, S. and Salajegheh, E. (2008). Optimal seismic design of steel structures by an efficient soft computing based algorithm. *Journal of Constructional Steel Research.* DOI: https://doi.org/10.1016/j.jcsr.2009.07.006

17. Kaveh, A. and Nasrollahi, A. (2014). Performance-based seismic design of steel frames utilizing charged system search optimization. *Applied Soft Computing.* DOI: https://doi.org/10.1016/j.asoc.2014.05.012

18. UC Regents. (2006). The open system for earthquake engineering simulation. Retrieved from http://opensees.berkeley.edu/OpenSees/home/about.php

19. Dorigo, M. (2008). Particle swarm optimization. *Scholarpedia*, 6(8):11472. DOI: doi:10.4249/scholarpedia.1486

20. Eberhart, R.C. and Shi, Y. (2001). Particle swarm optimization: developments, applications and resources. *Proc. Congress on Evolutionary Computation 2001*, Seoul, Korea. Piscataway, NJ: IEEE Service Center.

21. AISC (2014). Steel Construction Manual Fourteenth Edition. *American Institute of Steel Construction*. Chicago, IL.

22. Elnashai, S. and Sarno, L.D. (2008). Fundamentals of Earthquake Engineering. West Sussex, UK: John Wiley & Sons, Ltd.

23. Ericksen, J. (2007). Seismic Fuses. *Modern Steel Construction (Steelwise).* Retrieved from https://www.aisc.org/globalassets/modern-steel/steelwise/30765_steelwise.pdf

24. Megget, L.M. (2006). From brittle to ductile: 75 years of seismic design in New Zealand. *NZEE Annual Conference*. Retrieved from http://www.nzsee.org.nz/db/Bulletin/Archive/39(3)0158.pdf

25. Bachmann, H., Peter Linde, and Wenk, T. (1994). Capacity design and nonlinear dynamic analysis of earthquake-resistant structures. *10th European Conference on Earthquake Engineering (ECEE), Vienna*. DOI: 10.1002/eqe.4290231205

26. ASCE. (2010). Minimum Design Loads for Buildings and Other Structures, ASCE/SEI 7-10, Reston, VA. *American Society of Civil Engineers*, p. 72.

27. ASCE. (2010). Minimum Design Loads for Buildings and Other Structures, ASCE/SEI 7-10, Reston, VA. *American Society of Civil Engineers*, p. 90.

28. ASCE. (2010). Minimum Design Loads for Buildings and Other Structures, ASCE/SEI 7-10, Reston, VA. *American Society of Civil Engineers*, p. 66.

29. NEHRP. (2015). Recommended Seismic Provisions for New Buildings and Other Structures, FEMA P-1051/7-16, Washington, D.C. *National Earthquake Hazards Reduction Program.*

30. ASCE. (2010). Minimum Design Loads for Buildings and Other Structures, ASCE/SEI 7-10, Reston, VA. *American Society of Civil Engineers*, p. 89.

31. ASCE. (2010). Minimum Design Loads for Buildings and Other Structures, ASCE/SEI 7-10, Reston, VA. *American Society of Civil Engineers*, pp 91-92.

32. ASCE. (2010). Minimum Design Loads for Buildings and Other Structures, ASCE/SEI 7-10, Reston, VA. *American Society of Civil Engineers*, pp 104-105.

33. ASCE. (2010). Minimum Design Loads for Buildings and Other Structures, ASCE/SEI 7-10, Reston, VA. *American Society of Civil Engineers*, pp 92-93.

34. ASCE. (2010). Minimum Design Loads for Buildings and Other Structures, ASCE/SEI 7-10, Reston, VA. *American Society of Civil Engineers*, p. 97-98.

35. ASCE. (2010). Minimum Design Loads for Buildings and Other Structures, ASCE/SEI 7-10, Reston, VA. *American Society of Civil Engineers*, p. 161-162.

36. ASCE. (2010). Minimum Design Loads for Buildings and Other Structures, ASCE/SEI 7-10, Reston, VA. *American Society of Civil Engineers*, p. 162-163.

37. FEMA (2005). Improvement of Nonlinear Static Seismic Analysis Procedures, FEMA-440, Washington, D.C. *Federal Emergency Management Agency*.

38. Manjula, N.K., Nagaranjan, P., Pillia, M. (2013). A comparison of basic pushover methods. *Int. Refereed Journal of Engineering and Science (IRJES),* 2319-183X.

39. ASCE. (2006). Seismic Rehabilitation of Existing Structures, ASCE/SEI 41-06, Reston, VA. *American Society of Civil Engineers*.

40. Lagaros, Nikos D., Fragiadakis, M. (2010). Evaluation of ASCE-41, ATC-40, and N2 static pushover methods based on optimally designed buildings, *Soil Dynamics and Earthquake Engineering*. Elsevier: https://doi.org/10.1016/j.soildyn.2010.08.007

41. FEMA (2000). Prestandard and Commentary for the Seismic Rehabilitation of Buildings, FEMA-356, Washington, D.C. *Federal Emergency Management Agency*. p. 3-18.

42. FEMA (2000). Prestandard and Commentary for the Seismic Rehabilitation of Buildings, FEMA-356, Washington, D.C. *Federal Emergency Management Agency*. p. 3-19.

43. FEMA (2000). Prestandard and Commentary for the Seismic Rehabilitation of Buildings, FEMA-356, Washington, D.C. *Federal Emergency Management Agency*. p. 3-21.

44. FEMA (2000). Prestandard and Commentary for the Seismic Rehabilitation of Buildings, FEMA-356, Washington, D.C. *Federal Emergency Management Agency*. p. 1-32.

45. FEMA (2000). Prestandard and Commentary for the Seismic Rehabilitation of Buildings, FEMA-356, Washington, D.C. *Federal Emergency Management Agency*. p. 3-14.

46. FEMA (2000). Prestandard and Commentary for the Seismic Rehabilitation of Buildings, FEMA-356, Washington, D.C. *Federal Emergency Management Agency*. p. 5-33.

47. AISC (2010). Seismic Provisions for Structural Steel Buildings. ANSI/AISC 341-10, *American Institute of Steel Construction*. Chicago, IL.

48. FEMA (2010). Design Guide for Improving School Safety in Earthquakes, Floods, and High Winds, FEMA 424. Washington, D.C. *Federal Emergency Management Agency*.

49. FEMA (2006). Next-Generation Performance-Based Seismic Design Guidelines, FEMA-445. Washington, D.C. *Federal Emergency Management Agency*.

50. FEMA (2000). Prestandard and Commentary for the Seismic Rehabilitation of Buildings, FEMA-356, Washington, D.C. *Federal Emergency Management Agency*. p. 1-9.

51. FEMA (1997). NEHRP Commentary on the Guidelines for the Seismic Rehabilitation of Buildings, FEMA-274. Washington, D.C. *Federal Emergency Management Agency*. p. 2-4.

52. FEMA (2000). Prestandard and Commentary for the Seismic Rehabilitation of Buildings, FEMA-356, Washington, D.C. *Federal Emergency Management Agency*. p. 1-14.

53. He S, Wu QH ,Wen JY, Saunders, JR, Paton RC. (2004). An improved particle swarm optimizer for mechanical design optimization problems. *Eng Optimiz*, 35(5): 585-605.

54. Li, L.J. and Huang, Z.B. (2007). A heuristic particle swarm optimizer for optimization of pin connected structures. Computers & Structures. DOI: https://doi.org/10.1016/j.compstruc.2006.11.020

55. Dogan, E. and Saka, M.P. (2012). Optimum design of unbraced steel frames to LRFD-AISC using particle swarm optimization. *Advances in Engineering Software.* Computers & Structures. DOI: https://doi.org/10.1016/j.advengsoft.2011.05.008

56. Ohtori, Y., Christenson, R.E., and Spencer, Jr., B.F. (2004). Benchmark control problems for seismically excited nonlinear buildings. Notre Dame, IN. *Department of Civil Engineering and Geological Sciences, University of Notre Dame*: 46556-0767.

57. Hosseini G. and Kenarangi, H. (2012). OpenSees workshop. Retrieved from file:///C:/Users/pc/Downloads/OpenSeesWorkshopEng.Hoseini-Opensees%20(2).pdf

58. ASCE. (2010). Minimum Design Loads for Buildings and Other Structures, ASCE/SEI 7-10, Reston, VA. *American Society of Civil Engineers*, p. 2.

59. ASCE. (2010). Minimum Design Loads for Buildings and Other Structures, ASCE/SEI 7-10, Reston, VA. *American Society of Civil Engineers*, p. 5.

60. USGS (2014). U.S. Seismic Design Map Tools. *United States Geological Survey.* Retrieved from https://earthquake.usgs.gov/designmaps/us/application.php

61. ASCE. (2010). Minimum Design Loads for Buildings and Other Structures, ASCE/SEI 7-10, Reston, VA. *American Society of Civil Engineers*, pp. 73-77.

62. AISC (2010). Seismic Provisions for Structural Steel Buildings. ANSI/AISC 341-10. Chicago, IL. *American Institute of Steel Construction*, p. 9.1-63.

63. AISC (2010). Seismic Provisions for Structural Steel Buildings. ANSI/AISC 341-10. Chicago, IL. *American Institute of Steel Construction*, p. 9.1-200.

64. Chopra, A.K. (2011). Dynamics of Structures: Theory and Applications to Earthquake Engineering (Second ed.). Englewood Cliffs, NJ. Prentice Hall.

65. Wilson, E.L., Farhoomand, I., and Bathe K.J. (1973). Nonlinear Dynamic Analysis of Complex Structures. *University of California, Berkeley.* Retrieved from https://pdfs.semanticscholar.org/b736/91bb24486599b3b752ec14b241fed9eb8aac.pdf

66. Filippou, F. and Mazzoni, S. (2012). Steel02 material- Giuffré-Menegotto-Pinto model with isotropic strain hardening. Retrieved from http://opensees.berkeley.edu/wiki/index.php/Steel02_Material_--_Giuffr%C3%A9-Menegotto-Pinto_Model_with_Isotropic_Strain_Hardening

67. FEMA (2000). Prestandard and Commentary for the Seismic Rehabilitation of Buildings, FEMA-356, Washington, D.C. *Federal Emergency Management Agency*. p. 5-13.

68. Lignos, D.G. (2014), Modeling Steel Moment Resisting Frames with OpenSees. *OpenSees Workshop, University of California, Berkeley*. Retrieved from http://opensees.berkeley.edu/OpenSees/workshops/OpenSeesDays2014/SteelMomentFrames.pdf

69. FEMA. (2003). NEHRP Recommended Provisions for Seismic Regulations for New Buildings and Other Structures, FEMA 450-2, Washington, D.C. *Federal Emergency Management Agency*. p. 5-13.

70. SKGA. (2015). Basics of Seismic Design, Part 4- Performance Objectives. *S.K. Ghosh Associates LLC*. Retrieved from http://skghoshassociates.com/SKGAblog/viewpost.php?id=72

71. ASCE. (2010). Minimum Design Loads for Buildings and Other Structures, ASCE/SEI 7-10, Reston, VA. *American Society of Civil Engineers*, pp 73-77.

72. FEMA (2000). Prestandard and Commentary for the Seismic Rehabilitation of Buildings, FEMA-356, Washington, D.C. *Federal Emergency Management Agency*. pp. 5.40 – 5.44.

73. FEMA (2000). Prestandard and Commentary for the Seismic Rehabilitation of Buildings, FEMA-356, Washington, D.C. *Federal Emergency Management Agency*. pp. 5.5 – 5.7.